Privatdoz. Sven Barth

TECHNISCHE
UNIVERSITÄT
WIEN
Vienna University of Technology

Master thesis

Site-Selective Growth of Nanowires for Sensor-Applications

carried out at the

Institute of Materials Chemistry

Vienna University of Technology

under the supervision of

Privatdoz. Dipl.-Chem. Dr.rer.nat. Sven Barth

by

Lukas Hrachowina, BSc

Viktor Kaplan Str. 5c, 2362 Biedermannsdorf

Vienna, January 2017

Lukas Hrachowina

Acknowledgements

To begin with, I want to thank my supervisor Sven, for letting me independently work on such an interesting topic, yet always answering my questions and advising me.

Furthermore, I want to thank my colleagues for always being open to discussions and contributing ideas.

In addition, thank you…

…Felix for always putting on music in the lab.

…Michael for joking around and the exciting chess matches.

…Patrik for cheering me up when something did not work at the first attempt.

Thank you Patrik and Sven for acquiring more than a thousand SEM images.

Moreover, I cannot put into words how glad I am to have you on my side Aleks; thank you for always being patient with me.

Besides, I want to thank my parents for always supporting and listening to me.

And last but not least I want to thank my high school chemistry teacher Wolfgang, without whom I probably would not have studied chemistry.

Abstract

Tin(IV)oxide, germanium and tungsten(VI)oxide are semiconducting materials with resistance values depending on adsorbed molecules altering the space charge layer in proximity to the surface. Previous studies have shown the potential of these nanostructured materials in chemiresistor-based sensors. Especially nanowires stand out due to their excellent crystallinity and high surface area to volume ratio. They can be used in sensors as single-nanowire devices or as a network between electrodes. Nanowires can outperform other morphologies due to the few grain boundaries and the high surface-to-volume ratio. It is of advantage to integrate nanowires *in-situ* on the desired area, because it can be tedious and time-consuming to integrate them into electronic devices afterwards. Therefore, process parameters for the site-selective growth of tin(IV)oxide and germanium nanowires on micromembranes by use of low-pressure chemical vapour deposition (CVD) have been optimised. The deposition temperature and the precursor flux are crucial parameters to obtain the desired nanowire density and quality. Furthermore, the morphology of tungsten(VI)oxide nanostructures that were obtained by use of aerosol-assisted chemical vapour deposition has been investigated in order to obtain a reliable procedure for the growth in a cold wall CVD reactor. The efficient growth of nanowires requires a pre-treatment including the light induced ligand exchange in $W(CO)_6$. The gained knowledge on larger substrates has been used to achieve the site-selective deposition of tungsten oxide nanowires on micromembranes. The desired site-selective deposition of all three materials on one chip containing four micromembranes has been demonstrated. This is the first process, in which different materials are site-selectively deposited on a single chip. Additionally, experiments about the surface modification of nanowires with metal organic frameworks have been conducted and a setup has been constructed to allow liquid phase epitaxy of metal organic frameworks.

Kurzfassung

Zinn(IV)oxid, Germanium und Wolfram(VI)oxid sind halbleitende Materialien und können als gassensitive Resistoren für Sensormaterialien verwendet werden, deren Widerstand von adsorbierten Spezies an der Oberfläche abhängt. Die Nanostrukturierung solcher Chemiresistormaterialien kann hierbei die Sensitivität stark verbessern. Insbesondere Nanodrähte zeichnen sich durch ihre exzellente Kristallinität, gepaart mit hohem Oberflächen-zu-Volumen-Verhältnis aus. Nanodraht-basierte Sensoren können sowohl lediglich aus einem Einzeldraht, als auch aus einem Nanodrahtnetzwerk aufgebaut werden. Die Integration von Nanodrähten in elektronische Bauteile kann zeit- und arbeitsintensiv sein und es ist daher von Vorteil die Drähte an der gewünschten Stelle abzuscheiden und damit ebenfalls eine Verbindung von Elektroden zu erzeugen.

In dieser Arbeit wurden die Prozessparameter für das ortsselektive Wachstum von Zinn(IV)oxid- und Germanium-Nanodrähten mittels Niedrigdruck-Gasphasenabscheidung auf Mikromembranen optimiert. Dabei spielen sowohl die Abscheidetemperatur als auch der Precursorfluss eine große Rolle. Des Weiteren wurde die Morphologie von Wolfram(VI)oxid Nanostrukturen, die über Aerosol-unterstützte Gasphasenabscheidung gewonnen wurden, untersucht. Die kontrollierte und effiziente Synthese von Wolfram(VI)oxid-Nanodrähten in einem Kaltwandreaktor bedarf im ersten Schritt einen lichtinduzierten Ligandenaustausch. Durch das Anpassen der Prozessparameter konnten die gewonnen Erkenntnisse ebenfalls auf das ortsselektive Wachstum auf Mikromembranen übertragen werden. Die erwünschte Abscheidung von drei unterschiedlichen Nanodrahtmaterialien auf einem einzigen Chip konnte aufgrund der Vorarbeiten erzielt werden. Dies stellt das erste Verfahren des ortsselektiven Wachstums unterschiedlicher Materialien auf einem Chip dar. Des Weiteren wurden Versuche bezüglich der Oberflächenmodifikation von Nanodrähten mit metallorganischen Netzwerken durchgeführt und ein Versuchsaufbau realisiert, bei dem ein Substrat mit einem Roboterarm in unterschiedliche Lösungen eingetaucht werden kann um eine Flüssigphasenepitaxie von metallorganischen Netzwerken zu realisieren.

Table of Contents

1 Introduction

The dependence of resistance values on the surrounding gaseous environment of semiconducting oxides such as ZnO and SnO_2 was already described in 1962.[1] At that time, thin films and porous ceramics were used as gas-sensing devices and only few years later in 1968, first industrial products reached the market.[2] After 50 years of development the technology is rather mature with a library of gas-sensitive materials, but there is still plenty of room for improvement. Besides the material composition, the structure of those materials plays an important role and nanostructuring has led to the development of more sophisticated devices. Despite the large efforts in this area of research, metal oxide sensors still suffer from a poor selectivity, which complicates measurements under ambient conditions. One idea of improving the selectivity of gas-sensitive resistors is applying pattern recognition to the measured signals. Therefore, a sensor array is necessary and temperature gradients are applied to obtain more transducable information. However, operating devices at different temperatures has still limits in the differentiation between analytes, requires complicated readout and implicates limitations for low power devices.

However, the selectivity of a sensing device can be also improved by using more than one sensing material, in analogy to the non-selective biological receptors in the mammalian olfactory system. In order to express the resemblance to the operation of a nose, these artificial sensor arrays using pattern recognition to detect gaseous molecules are called electronic noses. Although electronic noses nowadays are not comparable to a human nose, they can quantitatively detect important gases in many fields of application and there are already industrial products available.[3]

As already mentioned, the usage of nanostructured materials helped to increase the sensitivity of such chemiresistors. For instance, nanowire-based devices have shown superior gas sensing behaviour when compared to their bulk counterparts, which is predominantly caused their high surface-to-volume ratio and their high crystallinity. However, the integration of nanowires into functional devices is time consuming and often includes several steps. One solution to this problem is the site-selective growth of the material and the *in-situ* contact formation to predefined electrodes. The operation of metal oxide gas sensors requires elevated temperatures for an effective detection of gases and therefore a heating source is required. Low power devices can be based on microhotplates, which can be used to induce *in-situ* localised nanowire growth and also to operate the sensor afterwards. This approach allows the formation of integrated circuits containing nanowire-based gas sensors.

Additional improvement to the selectivity of such sensors could be introduced by using a membrane covering the nanowires, so that only certain molecules reach the semiconducting surface. Latest results showed that some MOFs might be useful candidates for such membranes, especially ZIF-8 proved to be thermally as well as chemically stable enough to suffice the challenging requirements.[4]

1.1 Nanowires

Nanowires are defined as elongated crystals with a diameter between 1 and 100 nm.[5] Depending on their shape and aspect ratio they are also often called nanorods, nanobelts, nanofibers, whiskers, or nanoneedles as shown in Figure 1. Because two dimensions in such structures are limited to the nano-regime, they are often referred to as 1-dimensional or 1D structures.

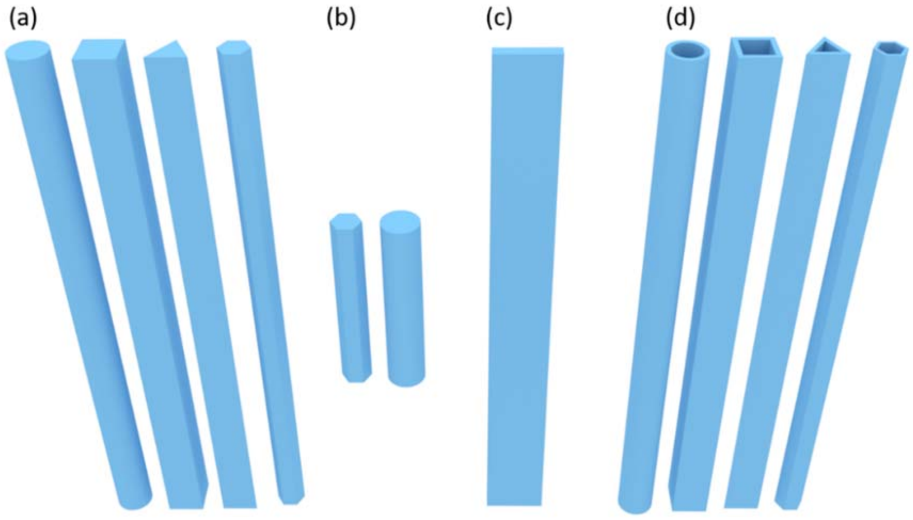

Figure 1: 1D structures with different cross-sections and aspect-ratios: (a) Nanowires, (b) Nanorods, (c) Nanobelt, (d) Nanotubes.

Nanowires have many advantages to their bulk counterparts, e.g. a much higher surface-to-volume ratio, but there are also new phenomena affiliated with the nano-regime like size-dependent excitation,[6] quantised conductance[7] and metal-insulator transitions.[8]

Nanowires can be used in many applications due to their excellent properties. Besides the use of nanowires as gas-sensitive resistors,[9-10] field effect transistors,[11] lasers,[12] light emitting diodes,[13] field-emission tips,[14] and solar cells[15] have been produced using nanowires. Furthermore, novel electrode materials have been made from silicon nanowires[16] and piezoelectric materials are used to produce 1D nanogenerators.[17]

There are in general two different approaches to synthesise nanowires: top-down and bottom-up. The most important top-down approach is chemical etching. While top-down approaches lead to nanowires with known orientation, very good crystallinity and low defect density, they often have a rough surface.

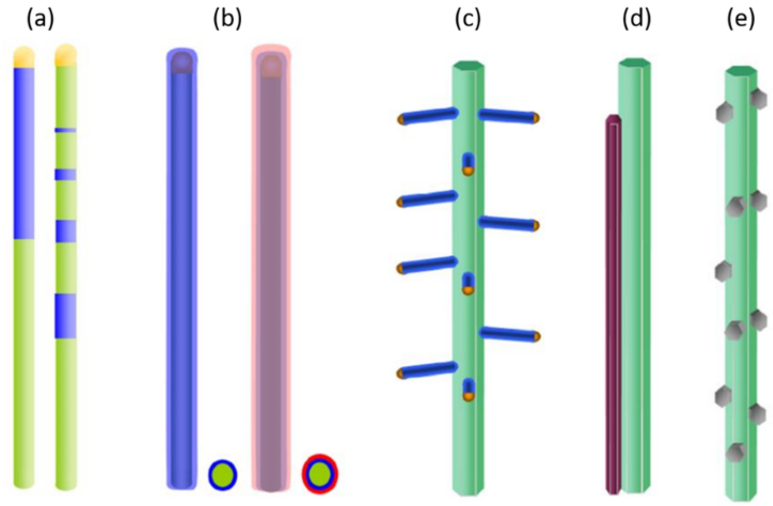

Figure 2: Different 1D heterostructures: (a) axial, (b) radial or coaxial, (c) branched, (d) aligned, (e) 1D-0D heterostructures.[18] *Reprinted with permission from Elsevier.*

The orientation of nanowires grown by the bottom-up approach is usually governed by the surface energy and the substrate can be used to predefine specific orientation. Moreover, the formation of heterostructures as shown in Figure 2 is enabled by simple process variation. The bottom-up syntheses also have some disadvantages including requirement of higher temperatures for the growth of certain materials, the incorporation of seed material in the growing nanowire can cause unintentional doping and post-growth techniques can be necessary to integrate the grown nanowires into functional devices. The post-growth alignment of nanowires can be achieved with a bubble-blow technique, in which the nanowires are aligned at the outer wall of a bubble due to their anisotropic shape,[19] or a dry transfer that enables sequential stacking,[20] or with dielectrophoresis, where nanowires are aligned onto prepatterned electrodes[21] for an effective integration in devices.

The method of choice for nanowire synthesis via the bottom-up approach is strongly dependent on the material. While some materials grow elongated nanocrystals because of their crystal structure, defects, or screw dislocations other materials need seeds to promote the formation of an elongated crystal. In addition, capping agents to restrain certain facets during the growth or the filling of a porous template can be used for nanowire synthesis.

Although conventionally nanowires are synthesised via gas phase, it is also possible to grow them from solution. Synthesis in solution enables the use of precursors that are not available for gas phase syntheses; however, the process can be more difficult to control due to the decreased diffusion length, that can cause secondary nucleation events and thus contamination of the material. Similarly to the processes described in 1.1.2. metal particles can be used as growth promoters leading to growth via the solution-liquid-solid “SLS”[22] or solution-solid-solid “SSS”[23] mechanisms.

1.1.1 Vapour-Solid Growth

Some materials tend to grow nanowires in gas phase syntheses due to their anisotropic crystal structure,[24] defects such as screw dislocations[25] or a self-catalytic formation of a metal wetting layer.[26] There is no additional seed needed, and therefore this mechanism is simply called vapour-solid growth, because the precursor is supplied via the gas phase and a solid nanowire grows. An advantage compared to metal seeded growth is that the nanowire cannot be doped by the seed material. On the downside, this growth is not applicable to all materials and this growth strategy often relies on defects in the crystal structure, which can be problematic for their use in devices.

Ideal crystals have atomically smooth surfaces and growth would be inhibited by the nucleation of surface steps and thus be very slow. However, real crystals have defects such as twin boundaries or screw-dislocations, causing preferred nucleation sites leading to a faster growth rate. Screw-dislocations have been treated theoretically[27] and a prominent example, where screw-dislocations induce the growth of mercury nanowires has already been reported in 1955.[25] A screw-dislocation can act as a promoter of 1D crystal formation and the growth of the crystal can helically occur parallel to the screw axis. There is always an exposed terrace, where new adatoms can nucleate due to the geometry of the staircase-like crystal structure (Figure 3a).

Although the geometric element of a twin-boundary is two-dimensional on the contrary to the one-dimensional geometric element of a screw-dislocation, it can induce nanowire growth. However, unlike screw-dislocations, twin-boundaries do not cause self-perpetuating steps and therefore new nucleation of steps is necessary (Figure 3b). Nevertheless, the edge of the twin-boundary is a preferred nucleation site on its own and nanowire growth thus occurs on the one side laterally, on the other side along the ridge of the twin boundary. Using *in-situ* TEM, such a growth of CuO nanowires has been successfully imaged.[28]

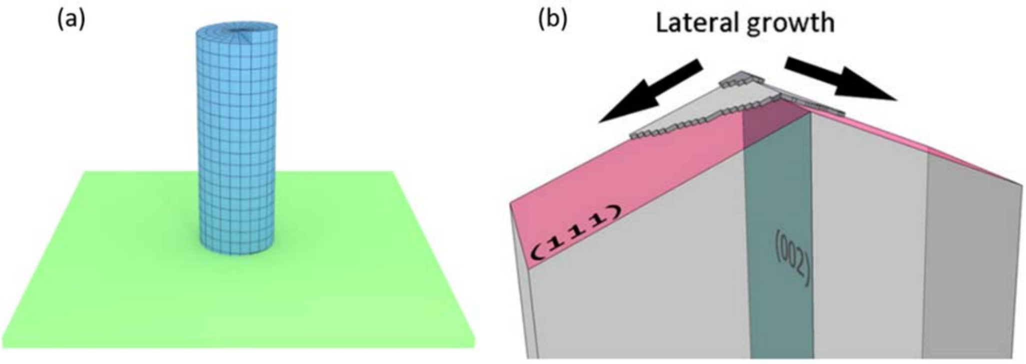

Figure 3: (a) Screw-dislocation leading to an elongated growth. New adatoms will always nucleate at the step, which leads to an elongated growth along the screw axis. (b) CuO nanowires can grow parallel to a (002) twin boundary, while new layers of (111) lattice planes are formed at the growth front.[28] *Reprinted with permission from American Chemical Society.*

Prominent examples for extraordinary anisotropic crystal structures are poly(sulphur nitride) that form a linear chain,[24] molybdenium chalcogenides[29] and the trigonal phase of selenium[30] and tellurium[31] as shown in Figure 4. The elongated growth is a result of the minimisation of surface energy.

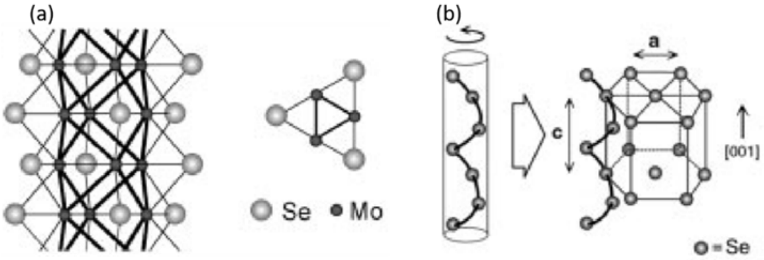

Figure 4: Anisotropic crystal structures: (a) Hexagonal close-packed linear chain of $Li_2Mo_6Se_6$ *and top view of the planar* $Mo_3Se_3^-$ *unit. (b) Crystal structure of t-Se. Helical chains of Se are hexagonally packed parallel to each other along the c-axis.*[5] *Reprinted with permission from Wiley-VCH.*

1.1.2 Vapour-Liquid-Solid Growth

In a vapour-liquid-solid (VLS) growth, that has already been described in 1964 by Wagner and Ellis, the precursor is supplied via the gas phase and decomposed at a liquid metal seed droplet.[32] In fact, the seed may be solid at first, but melts due to the formation of a low melting alloy of eutectic composition. Further increase in the decomposing material content leads to a supersaturation of the droplet and subsequent nucleation of the material via precipitation at the alloy-substrate interface. Figure 5a exemplarily shows the Au-Ge binary phase diagram, in which these processes are easy to comprehend. However, predictions are difficult for more complex systems, in which ternary or quaternary phase diagrams would be required, that are most often not available. The nanowire grows as long as precursor is supplied via the gas phase as shown in Figure 5b.

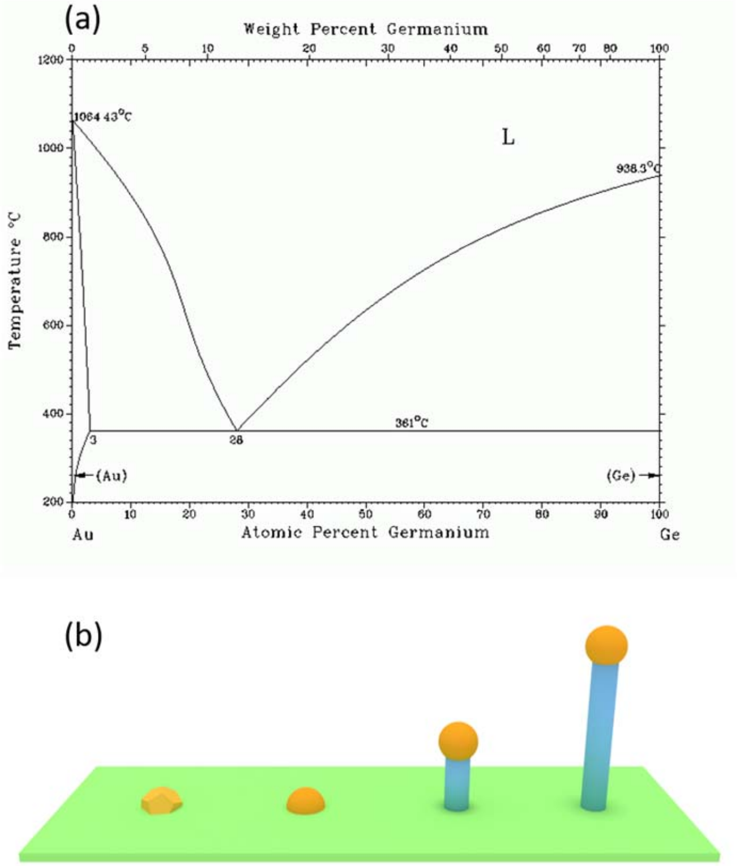

Figure 5: (a) Exemplary Au-Ge phase diagram. After heating to 450 °C the gold seed is still solid. By supplying Germanium via the gas phase, an alloy is formed and the Germanium amount in the solid seed is increased. When no more Germanium is soluble in the solid seed, the seed melts. In the liquid phase the Germanium amount is further increased until oversaturation leads to precipitation of a Germanium nanowire.[33] Reprinted with permission from Springer. (b) Scheme of the VLS-mechanism. Solid seed melts due to rise in temperature and dissolution of the nanowire material in the seed. Oversaturation in the liquid droplet leads to nucleation of the nanowire that grows until no further precursor is supplied via the gas-phase.

The VLS mechanism is in principle applicable to all materials, if an adequate seed is found. To grow pure nanowires, very low solubility of the seed in the nanowire material is indispensable; however, sometimes the seed material is intentionally incorporated into the nanowire material. This procedure allows to form elongated crystals of metastable alloys exceeding the thermodynamic solubility limit.[34-35]

1.2 Chemical Vapour Deposition

A convenient method to prepare nanowires, but also other nanostructured thin films is chemical vapour deposition (CVD). CVD involves a chemical reaction or decomposition of a precursor that is supplied via the gas phase on a surface. A CVD reactor with direct heating of a substrate or a susceptor containing the substrate, e.g. inductive heating of a metal or a graphite susceptor, is called a cold wall reactor. In contrast, an assembly where the whole deposition zone is heated indirectly using a furnace, is called a hot wall CVD reactor. While hot wall reactors are most often cheaper and generate a uniform temperature distribution, they have a lower deposition efficiency, because the heated wall of the reactor causes the same reaction that should occur at the substrate and is thus also coated. A cold wall reactor avoids this problem, allows better control of the deposition and avoids contamination from deposits originating at the reactor walls. Both variations can be used under different pressures from 10^{-6} mbar to atmospheric pressure. Besides thermally induced processes, the energy required for the chemical reaction can be supplied by a plasma or a light source. The reactions occurring during the CVD process are as diverse as the precursors used for CVD. Halides, hydrides, metal carbonyls or other metalorganic precursors are used for thermal decomposition. Moreover, additional reducing or oxidising agents can promote the respective reductions or oxidations to form the desired deposit. The use of precursor mixtures for the deposition of complex materials can be challenging due to complications resulting from different vaporisation rates and decomposition temperatures. An approach to better control the stoichiometry and reduce the number of parameters governing the CVD process is the use of single-source precursors, which are molecular species containing all components of the desired material.

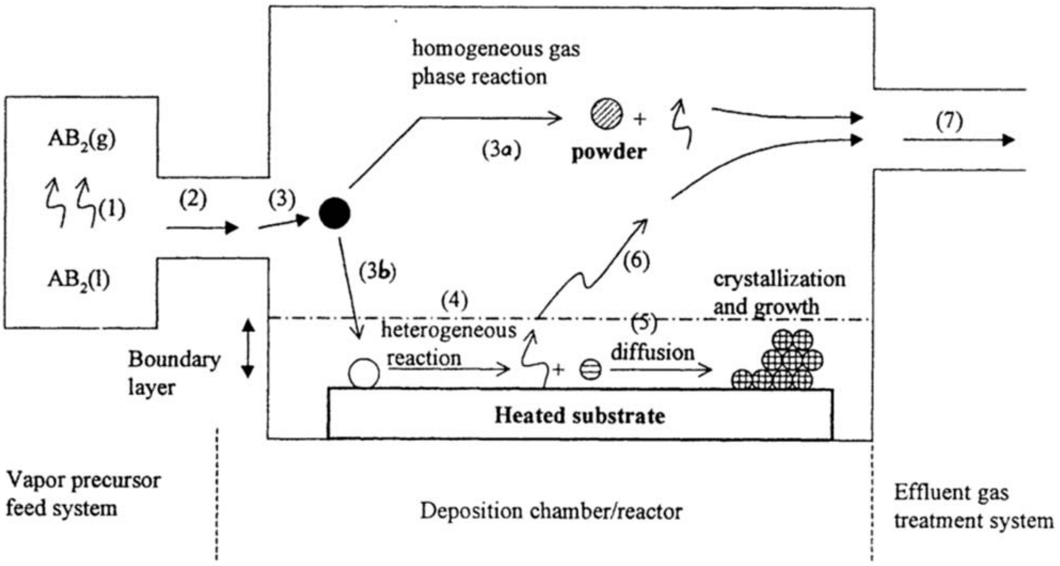

Figure 6: Scheme of a CVD process. Individual steps are discussed in the text.[36] *Reprinted with permission from Elsevier.*

In general, a CVD process may be divided in following schematic steps:

1. Generation of the gaseous precursor.
2. Transport of the precursor into the reaction chamber.
3. Formation of intermediate species
    3.1. At high temperatures in the reactor, the precursor reacts in a homogenous gas phase reaction before reaching the substrate. The formed powder may be collected at the substrate and acts as nucleation seed.
    3.2. Via diffusion and/or convection the precursor reaches the surface of the substrate, where the following steps proceed.
4. Adsorption to the heated surface causes a heterogenous reaction depositing the desired material and forming volatile by-products.
5. Diffusion of the deposit on the surface form nucleation centres that cause the formation of a film.
6. Volatile by-products are removed from the surface of the substrate by diffusion and convection.
7. Unreacted precursor and by-products are removed from the reaction chamber.

There are three simple models explaining the nucleation of thin films, when epitaxial growth is targeted. In case the adatom preferentially nucleates at the substrate, i.e. the sum of the epilayer surface energy and the interface energy is smaller than the substrate surface energy, a monolayer of the thin film is deposited first, followed by further layers of the deposited film. This layer-by-layer growth is named after Frank van der Merwe. The contrary extreme is the Volmer-Weber growth, where the substrate surface energy is big compared to the interface energy and the epilayer surface energy, which causes the growth of isolated islands. However, despite of a small interface energy, a monolayer might be deposited first, if the epilayer is strained. After initial layer-by-layer growth, islands are formed to relax the strain. This mechanism is called Stranski-Krastanov growth mode.

Unless precursors with high vapour pressure are used, the initial step of generating an active precursor in the gas phase is not trivial. There are different approaches to this problem and in fact, one way to classify CVD processes is the different solution to this.

1.2.1 LPCVD

Low pressure-CVD is applied to volatile liquid or solid precursors but can also be carried out with gaseous precursors. Typically, LPCVD is operating between 0.1 and 10 mbar. If the pressure is smaller than 0.0001 mbar, one speaks of ultrahigh-vacuum CVD (UHVCVD). In fact, the only difference regarding the process is a change of the rate limiting step of the deposition. While CVD under atmospheric pressure is mass transport or diffusion limited, the reduction of pressure causes a much higher mass transfer rate and the deposition is typically limited by the surface reaction rate. However, temperature changes also affect the deposition characteristics.

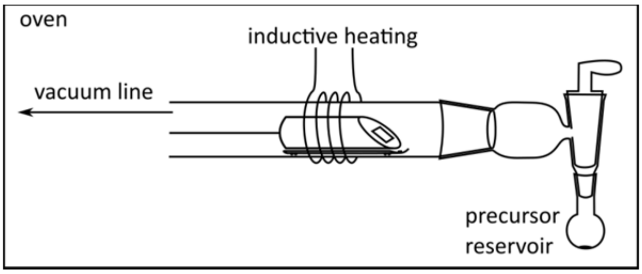

Figure 7: Possible cold wall LPCVD setup. The substrate is attached to a graphite susceptor that is inductively heated; temperature is controlled with a probe. The solid or liquid precursor is placed in a flask and a valve is used to start and stop the precursor flow.

1.2.2 AACVD

A big advantage of aerosol-assisted-CVD is the independence on the precursors volatility. In this process an aerosol of a solution containing the precursor is generated and transported to the substrate with a carrier gas. In the reaction chamber the solvent evaporates and thus the active species in the gas phase of the non-volatile precursor is generated. Typically, the solvent and carrier gas used are inert, but sometimes they are used as reducing or oxidising agents, reacting with the precursor, e.g. when using compressed air as carrier gas as well as oxidising agent.

Because of the simplification of the generation of the gaseous precursor, without the need of a vacuum system, AACVD is a very cheap type of CVD apparatus.

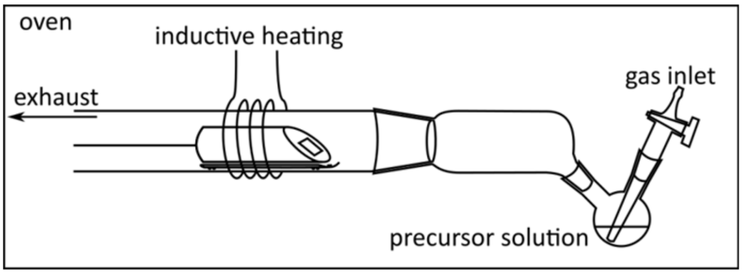

Figure 8: Possible cold wall AACVD setup. The substrate is attached to a graphite susceptor that is inductively heated; temperature is controlled with a probe. The precursor solution is placed in a two-necked flask and a carrier gas is bubbled into the solution. Not shown in the scheme is the ultrasonic humidifier that is placed below the flask to generate the aerosol that is then transported with the carrier gas to the substrate.

1.3 Metal-Organic Frameworks

Metal-Organic Frameworks (MOFs) are crystalline solids with a high specific surface that consist of metal-containing connectors, so called secondary building units (SBU), which are bonded by organic linkers, so that a two- or three-dimensional network is formed (Figure 9).[37-39] These coordination polymers are of extraordinary interest because the high porosity and the possibility of tuning the properties by modification of the organic linkers and/or the SBUs lead to an extremely broad range of applications e.g. as materials for gas storage,[40-42] membranes,[43] sensors,[44-45] and catalysts.[46] Another option to further improve the desired qualities of the MOF is a postsynthetic modification, by covalent modification of functional linkers, coordinate covalent modification of the connectors, or a combinational strategy in which the functionality of the linker is changed so that coordinate covalent modification is possible afterwards.[47]

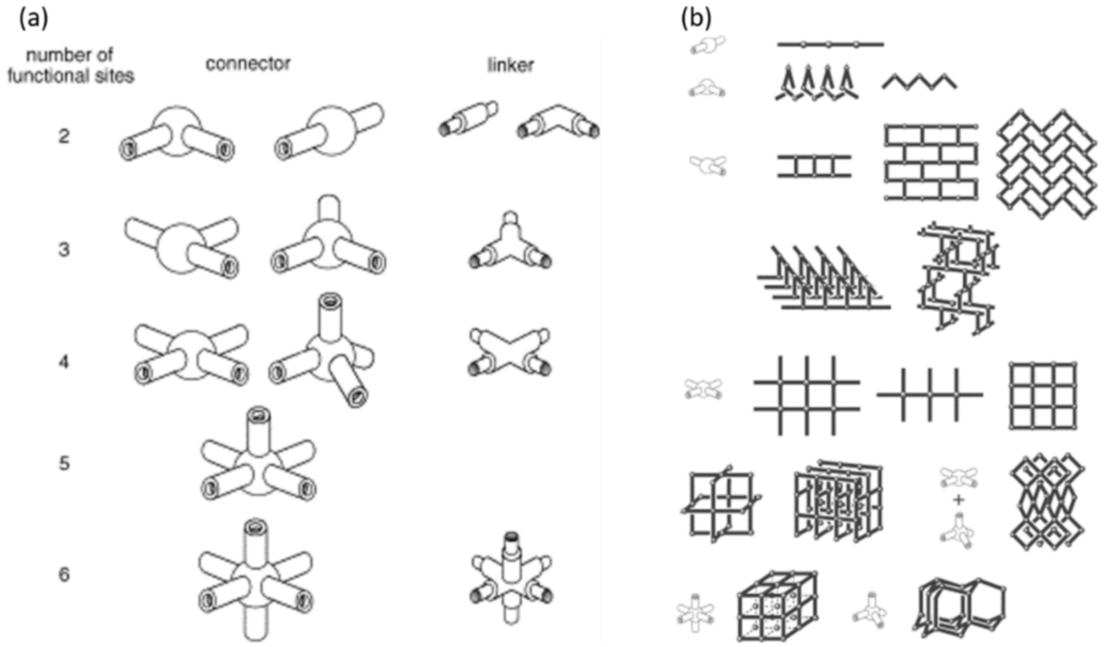

Figure 9: (a) Possible connectors and linkers with different numbers of functional sites. (b) Diversity of structures by combining different connectors only with linear linkers. A multitude of more complex structures are possible by using other linkers.[48] Reprinted with permission from Wiley-VCH.

Although graphical illustrations of MOFs often depict their structure as a triviality, it is actually not easy to correctly predict. To avoid further complications, very often rigid ligands are used as linkers, so that the possibilities of building different periodic networks are restricted.

As there are no proper IUPAC-endorsed names for MOFs and a systematic nomenclature still has to be developed, many MOFs are known under trivial names, which normally consist of abbreviating letters depending on the research group, followed by numbers.[49] These abbreviations include names as: MOF, IRMOF, HKUST, MIL, NOTT, ZIF, etc.

1.3.1 Typical Syntheses

MOFs are very diverse regarding their connectors, linkers, and structure and as diverse are the possible ways to synthesise them. While some MOFs can be synthesised at room temperature just by mixing of the ligands and the metal ion,[50] others need to be heated either conventionally[51] or by microwave.[52] Additionally, electrochemical[53] and mechanochemical[54] approaches, as well as ultrasonic methods[55] have been implemented. Nowadays, some MOFs are commercially available. Although the layer-by-layer growth[56] is rather a niche method only capable of producing thin films, this synthesis shall be investigated in detail besides conventional synthesis, because this work mainly focusses on the surface modification of nanowires.

The layer-by-layer (LBL) growth (Figure 10) is using a liquid epitaxy approach to grow a thin MOF film on a self-assembled monolayer (SAM).[56] MOFs grown with this method are often called SURMOFs to emphasise, that the MOF was grown on a surface. The best examined model for SAMs are thiols on gold surfaces and most SURMOFs are grown on gold,[56-58] but there were also other substrates used for the LBL growth in literature.[59-60] The SAMs used are functionalised with alcohols, carboxylic acids, or other functional groups where the SBUs of the MOF can be bonded. The SAM-functionalised substrates are successively immersed into solutions containing the SBU and the linker of the MOF. Between each layer a washing step in the pure solvent is implemented, to clean the surface of excessive molecules.

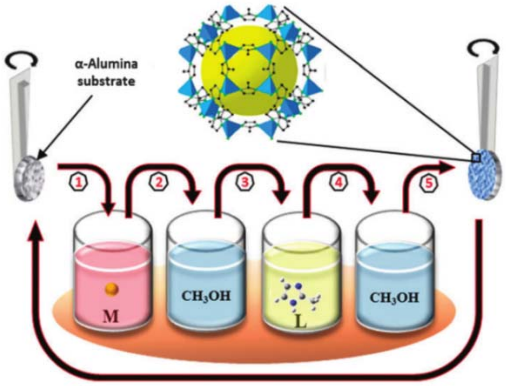

Figure 10: LBL scheme for the growth of a ZIF-8 layer on α-Alumina. The substrate is immersed into solutions containing the metal SBU and the organic linker. In between, washing steps in methanol are implemented.[60] Reprinted with permission from Royal Society of Chemistry.

By using the layer-by-layer method, interpenetration is avoided and different orientations of the SURMOF can be obtained by using different functionalised SAMs.[58]

1.3.2 ZIF-8

Zeolitic imidazolate frameworks are a certain subgroup of MOFs with zinc(II) or cobalt(II) centres. In this case, eponymic are the linkers and the resulting structural motifs. The crystal structures of the MOFs can be related to conventional zeolites due to the similarity of the imidazole linkers leading to the same bridging angle of 145° as in zeolites (Figure 11).

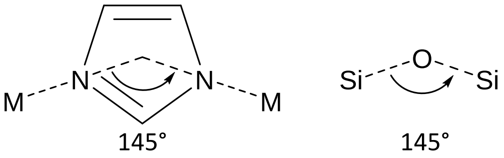

Figure 11: Bridging angle of 145° in ZIFs and zeolites.

ZIF-8 is obtained by using Zn^{2+} as SBU with 2-methylimidazole as linker. Single crystal X-ray diffraction of ZIF-8 crystals reveal a sodalite I-43m crystal structure with large cavities of 11.6 Å, as shown in Figure 12.

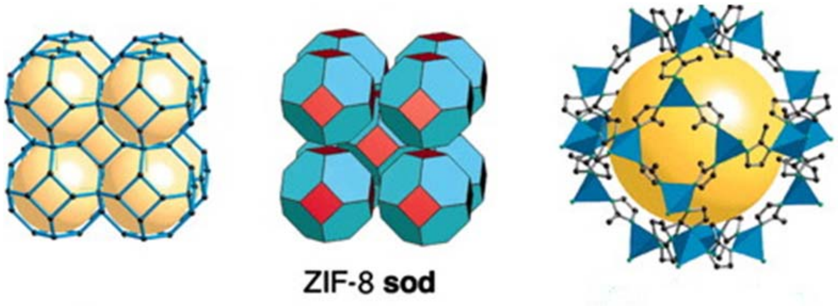

Figure 12: Single crystal x-ray structure of ZIF-8. 2-methylimidazole is connected with blue ZnN_4 tetrahedrons. The yellow sphere represents the cavity of the structure.[4] Reprinted with permission from National Academy of Sciences.

ZIF-8 is available by different synthetic approaches. Highly crystalline ZIF-8 was obtained by heating a solution of zinc(II)nitrate and 2-methylimidazole in dimethylformamide to 140 °C for 24 h, but it can even be obtained by precipitation after adding zin(II)nitrate to a 2-methylimidazole solution at room temperature. ZIF-8 can furthermore be grown using the layer-by-layer method via liquid phase epitaxy on a SAM. For instance, a [110]-oriented ZIF-8 film could be grown using a hydroxyl-terminated SAM.[61]

Thermogravimetric analysis of ZIF-8 shows a weight loss of 28.35 % until 450 °C, followed by a plateau until 550 °C. Although the sample turned black afterwards, Park *et al.* claim that the MOF is maintained verified with XRD and that the darkening of colour happens due to carbonisation of guest molecules. ZIF-8 is also chemically very inert and withstands several days in boiling benzene, methanol and water and 24 h in refluxing aqueous NaOH solution, which has been shown in an XRD-based study.[4]

1.4 Gas-Sensitive Resistors

Most materials used as gas-sensitive resistors are semiconductors and typically metal oxides are used. The conductivity of the semiconductor changes, because adsorbed molecules on the surface of a semiconductor change the electron density at the surface and thus the space charge layer. In general, there are two types of semiconductors. In n-type semiconductors electrons are the majority charge carriers, while in p-type semiconductors positively charged holes are the majority charge carriers. Gas molecules can be divided into oxidising and reducing gases. For a p-type semiconductor, the conductivity increases in presence of oxidising gases and decreases in presence of reducing gases, while n-type semiconductors behave inverse. Because the resistance can be easily and very fast measured, this is a convenient way to sense gaseous molecules.

Table 1: Change of resistance of semiconductors interacting with gas molecules.

	oxidising gases	reducing gases
n-type	+	−
p-type	−	+

Although the qualitative explanation of the sensor response is easily rationally explained, the exact mechanism in gaseous mixtures has to be verified in operando experiments due to the complexity of adsorbed species at the semiconductors surfaces. For example, ionosorbed oxygen may appear as O_2^-, O^-, or O^{2-} depending on the temperature. Between 250 and 400 °C, which is the most important temperature regime for gas sensing with metal oxide semiconductors, O^- is dominating as shown for SnO_2.[62] Inflammable gases often react with ionosorbed oxygen species, which explains, why the sensibility of some metal oxide sensors is worse under nitrogen than under ambient conditions. At n-type semiconductors the main charge carrier – electrons – are locked at the surface by the chemisorbed oxygen, therefore the resistance increases:

$$O_2 + 2e^- + 2* \rightarrow 2\,O^- \tag{1}$$

At a p-type semiconductor charge carriers – positive holes – are produced by chemisorbing oxygen, which leads to a decrease of resistance:

$$O_2 + 2* \rightarrow 2O^- + 2h^+ \tag{2}$$

In addition, humidity dependent hydroxyl groups at the surface can induce further reaction channels and thus data evaluation is complicated. Corrected data can be obtained using equipment, which can be used for investigations under operando conditions. These are only two of the gaseous species involved in the sensing in realistic atmospheres and many intermediate compounds have to be considered. A tremendous amount of effort has been put into investigating the sensitivity and selectivity of all kinds of metal oxides to different gases, but especially regarding sensitivity, the morphology of the material is probably even more important.[9, 63] To optimise sensitivity, the resistance of grain boundaries has to be minimised and the surface-to-volume ration maximised. Therefore, porous films were improved by synthesising nanocrystalline films, where the grain size is no greater than two times the Debye-length λ_D, so that the electric potential affects the whole grain.[62] Even better properties have been found in semiconducting nanowires.[9]

1.4.1 Tin Oxide

Although SnO_2 is the most prominent tin oxide, SnO, Sn_2O_3 and Sn_3O_4 are also known. Tin(IV)oxide is one of the most investigated gas sensor material. It is a large bandgap (3.6 eV) n-type semiconductor due to intrinsic oxygen vacancies and chemically inert. Although SnO_2 is polymorph, it preferentially crystallises in the rutile phase $P4_2/mnm$, but at high pressures an orthorhombic phase is obtained.

Besides its use as solid state gas sensor, SnO_2 can be used as transparent conductive oxide (TCO)[64] either as indium-tin-oxide (ITO) or fluorine-doped SnO_2. Tin(IV)oxide can be used as coating for windows to inhibit heat exchange because SnO_2 is transparent for visible light, but highly reflective for infrared light.[65] Another application for SnO_2 coated windows is the use of its transparent but conductive properties for electrochromic windows that change their colour or transparency by applying a voltage.[66] Moreover, SnO_2 exhibits catalytically properties and is used in heterogenous catalysis. For instance, adding copper and chromium to SnO_2 catalysts their performance can compete with Pt/Al_2O_3 for automotive catalyst applications.[67]

As gas-sensitive resistor, SnO_2 is sensible to NH_3, NO_2 and ethanol and many more gases, but it is best known as CO-sensor. CO is oxidised by ionosorbed oxygen species on the SnO_2 surface, thus decreasing the resistance. As SnO_2 sensors are typically operated at temperatures, where O^- are the dominant oxygen species, following reaction (3) takes place:

$$CO_{(g)} + O^-_{(ads)} \rightleftharpoons CO_{2(g)} + e^- + * \tag{3}$$

NO_2 is an oxidising gas and SnO_2 a n-type semiconductor, therefore the resistance of the SnO_2 increases in the presence of this gas. The effect can further be explained by the fact that NO_2 adsorbs at an oxygen vacancy, whereby it traps an electron and thus reduces the charge carrier density, as shown in (4).

$$NO_{2(g)} + e^- + * \rightleftharpoons NO^-_{2(ads)} \tag{4}$$

On the other side, while NH_3 decreases the resistance of SnO_2 because it is a reducing gas, the mechanism causing the change in conductivity is harder to understand, as three competitive reactions may take place at the surface and furthermore the measurement is strongly dependent on relative humidity, indicating that adsorbed OH groups at the surface affect the surface reactions of NH_3.

SnO_2 nanowires can be grown with LPCVD via a VLS mechanism using alkoxide precursors and gold as seed material.[68] The nanowires can be grown epitaxially on TiO_2[69] and form random networks on other surfaces. Additionally, SnO_2 nanowires are obtained by oxidising tin vapour[70] and by evaporation of SnO.[71]

1.4.2 Tungsten Oxide

While WO_3 can be described by WO_6 octahedrons that are linked via vertices, WO_2 can be described via WO_6 octahedrons linked via edges. By linking WO_6 octahedrons via vertices as well as edges an enormous variety of suboxides including W_2O_5, $W_{18}O_{49}$, W_3O_8, W_5O_{14}, and $WO_{2.9}$ exists. In some of these suboxides, tungsten is fourfold or sevenfold coordinated by oxygen. As diverse the tungsten suboxides and their crystal structures are, as many morphologies have been reported, including nanotubes,[72] nanobelts,[73] nanorods[74] and nanowires.[75] WO_3 is an n-type semiconductor and band gaps varying from 2.6 to 3.0 eV[76] have been reported.

WO_3 is used in smart windows because of its electrochromic properties.[77] In addition, WO_3 can be used for water splitting due to its photoelectrocatalytical properties.[78]

WO_3 is a n-type semiconductor and the fundamental concept of resistance change are very similar to SnO_2 as discussed in section 1.4.1. WO_3 does not seem to be very sensitive to any specific gas, but sensibility towards NO_x, O_3, H_2S, SO_2, H_2, and NH_3 have been reported.

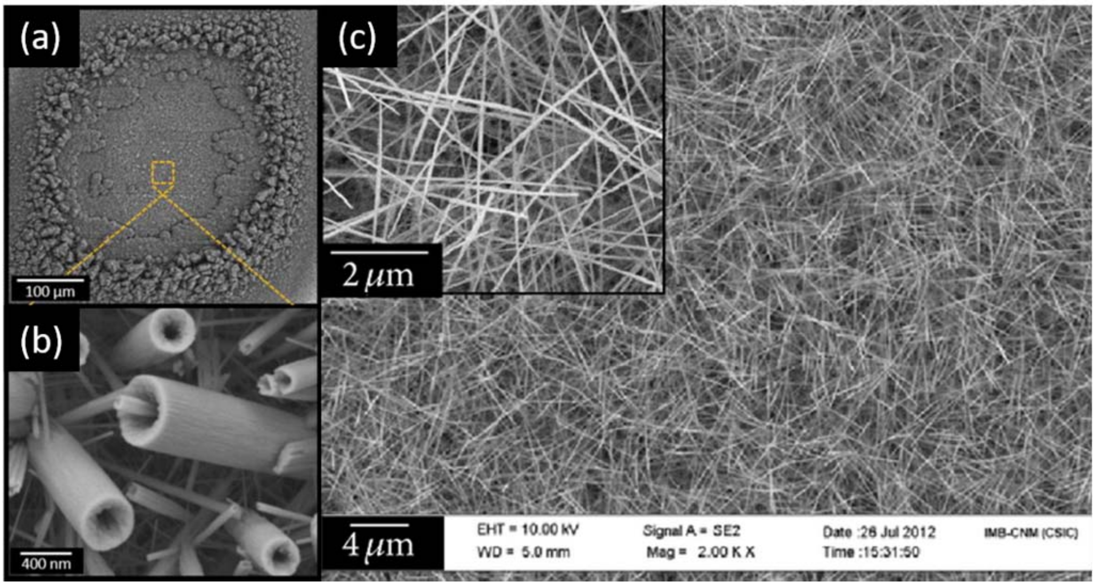

Figure 13: (a) Inhomogeneous deposition of WO_{3-x} nanostructures on a micromembrane. (b) Higher magnification provides evidence of a mixture of nanotubes and nanowires.[79] Reprinted with permission from Elsevier. (c) WO_{3-x} nanowires grown in a hot wall oven.[80]

Polycrystalline films of WO_3 have been prepared using dc magnetron,[81] ion-beam[82] or rf sputtering[83] of pure tungsten or tungsten oxide targets. Formation of nanowires via a VS-growth has been reported for tungsten suboxides such as $WO_{2.77}$[84] or $W_{18}O_{49}$[85] prepared via AACVD. Figure 13 shows the site-selective, but inhomogeneous deposition of mixed WO_{3-x} nanostructures[79] from a cold wall setup (Figure 13a and b) in comparison with the WO_{3-x} nanowires[80] obtained in a hot wall process (Figure 13c). The differences between cold wall and hot wall setups and their consequences for deposition WO_{3-x} nanostructures will further be discussed in section 3.3.

1.4.3 Germanium

Germanium is a p-type semiconductor with a band gap of 0.67 eV that crystallises in a cubic diamond structure. Hexagonal germanium is also known and desired due to its direct band gap in contrary to pure cubic germanium, which is an indirect semiconductor. However, it was possible to turn cubic germanium into a direct band gap semiconductor with straining, either mechanically[86] or intrinsically via doping with tin.[34-35]

Germanium has superior electrical properties compared to silicon, e.g. a higher carrier mobility, causing an increased interest of researchers in the last decade. However, the oxidation of germanium surfaces is problematic, because GeO_2 is not as stable as SiO_2 and soluble in water. Hence, alternative surface passivation is desired. More recent research has led to the use of germanium nanowires in field effect transistors,[87] anode material in lithium batteries,[88] and photoresistors.[89]

It is hard to control the oxidation of germanium, when it is used as a gas-sensitive resistor and therefore, it is hardly used for this purpose. Still, germanium nano-clusters have been reported as humidity and hydrogen sensor.[90] More recently, germanium nanowires have been reported as gas sensing device, which will be discussed in a separate chapter 3.2.[91]

Germanium nanowires are typically synthesised via CVD, using gold seeds and germane precursors,[92] but they are also obtainable from metal seeded reactions in supercritical fluids[93] or solutions.[94] Furthermore, pulsed laser deposition[95] and thermal evaporation of germanium[96] are used to produce 1D Ge structures. Additionally, germanium nanowires are available via template techniques using mesoporous silica[97] and electrochemical etching.[98]

1.4.4 Electronic Nose

The mammalian olfactory system is extremely sensitive and can detect various odours even at low concentrations. No wonder, dogs are trained and used to detect explosives and drugs. The first approach imitating a mammalian nose used three different metal oxide semiconductor transducers to detect several odours without selective sensors via pattern recognition.[99] After more than 30 years of research an electronic device that is comparable to the mammalian olfactory system still has not been developed, but the electronic nose that has emerged from this research is not inferior, it just has a different field of application. Nowadays electronic noses may not be able to smell odours like the human nose, but they are capable of detecting important odourless gases like CO, CO_2, NO_x, H_2O or VOCs.[100]

Probably because an array of sensors best resembles the mammalian olfactory system, this setup is still most often used. Still, metal oxide sensors are regarded as the standard sensor in electronic noses, but also surface or bulk acoustic wave sensors[101] and conducting polymer sensors[102] are used. Although one might think, that by combining all available sensors the optimal selectivity is generated, in fact the noise is amplified by increasing dimensionality of the sensor array. It is therefore important to select few, adequate sensors to obtain a useful device.[3]

But, besides the typical sensor arrays, new approaches to an electronic nose have been made, using optical sensor systems, mass spectrometry, ion mobility spectrometry, gas chromatography or infrared spectroscopy. A combination of different technologies is also possible, although further increasing the complexity and costs of the setup, and is commercially available.[100] In Figure 14 an example of an electronic nose is shown, that uses a temperature gradient to enhance the discrimination power of the device.[103]

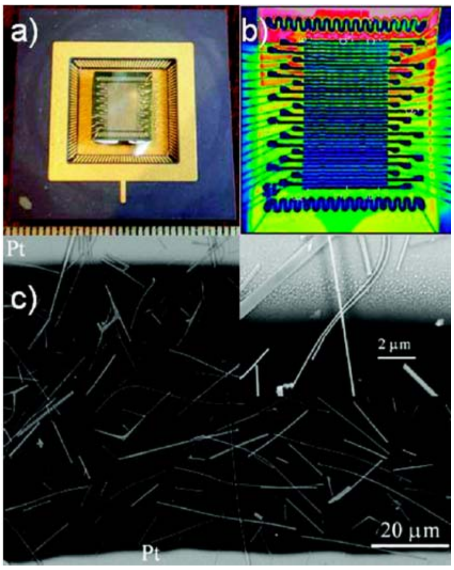

Figure 14 (a) A gradient microarray electronic nose. (b) An IR image of the array visualises the temperature gradient. (c) SEM image of SnO_2 nanowires between two Pt electrodes.[103] Printed with permission from American Chemical Society.

2 Motivation and Research Goal

SnO_2 nanowires have been grown at micromembranes before, however the low amount or absence of a 2D layer was not explained in detail. In addition, the site-selective growth of Ge nanowires has been demonstrated on microhotplates before, but these devices are only stable up to ~450 °C and therefore not suitable for the deposition of tin oxide. For this purpose, the deposition on micromembranes requires optimisation to ensure an optimal nanowire deposit. Tungsten oxide nanowires have not yet been homogeneously deposited site-selectively. The only report on the site-selective deposition of 1D tungsten oxide showed inhomogeneous deposition of material and also the morphology of the oxide deposit varied from nanowires to nanotubes.[79]

Using a cold wall CVD setup, the morphology of WO_{3-x} nanowires could be optimised and the gained knowledge could be transferred to site-selectively grow nanowires on micromembranes. The process developed in this thesis should allow the deposition of different nanowires on one chip. The targeted nanowire materials in this study are SnO_2, Ge and WO_3.

Although many metal oxide sensors are very sensitive, their selectivity is in great need of improvement. With the use of pattern recognition applied to an array of sensor materials, a more sophisticated selectivity is achieved, but one way to even further improve the selectivity is the implementation of an integrated membrane, creating a hybrid material. MOFs are very versatile porous materials and there are many candidates that are thermally as well as chemically stable robust enough to be used as a membrane in metal oxide sensors. When deposited on nanowires as a thin film, a core-shell structure is obtained, that combines the sensitivity of the nanostructured chemiresistor with an improved selectivity, because only gases that are small enough to pass the pores of the MOF can adsorb on the surface and change the resistance. Therefore, first deposition setups are set up in this thesis and tested for their actual use of MOF layer growth.

3 Results and Discussion

Nanowires possess superior properties compared to their bulk counterparts. For instance, the high surface-to-volume ratio paired with high crystallinity in nanowires is important for applications in resistor based gas sensing, which generally relies on diffusion effects influencing the response times and also the active surface for an effective interaction of adsorbates. In addition, typically the total resistance is smaller when compared to nanoparticle-based devices, due to the good crystallinity of nanowires and a reduced number of grain boundaries in the percolation paths.

One of the major challenges for the use of nanowires in functional devices is the integration procedure, which often relies on the transfer, positioning and contact formation of either a single nanowire or multiples. Another way to use them is in form of a mesh, in which the nanowires contact each other. The use of nanowire meshes usually require the heating of the larger substrate for the chemiresistor operation. A low power-solution to prepare sensor devices containing nanowire networks is the site-specific growth on heated micromembranes using thermally induced CVD.[10] The local heat source exclusively triggers the decomposition of the precursor and facilitates the growth of inorganic nanostructures such as nanowires without the contamination of the surrounding substrate. This method to grow nanowires is compatible with standard chip processing technologies and integrated circuits using nanowires as functional devices can be produced. The nanowires bridge the gap between pre-patterned interdigitated electrodes on top of the membrane and thus an *in-situ* integration can be achieved. In regard of electronic noses, it would be possible to create one single chip containing a sensor array and the electronics required for pattern recognition, while also lowering production costs.

The micromembranes used in this study are already described in literature.[104] A 400 times 400 µm spiral-shaped polysilicon heater is placed on a Si_3N_4 membrane and electrically isolated by a SiO_2 layer, on top of which interdigitated platinum electrodes are placed as can be seen in Figure 15. Four such membranes are placed on one TO-8 package. The nanowire network grown on those membranes closes the circuit between the interdigitated electrodes and the resistance can be measured. An advantage of this setup compared to others[105] is that the circuit for heating is independent of the circuit for measuring the resistance. The temperature of the devices is precisely adjusted via Joule heating by applying a DC voltage. However, one drawback is the not calibrated pressure dependence of the resistance, which leads to higher temperatures at reduced pressures complicating LPCVD processes.

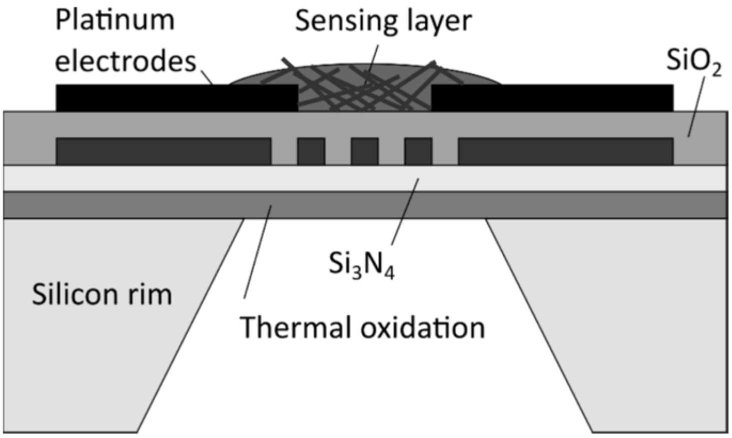

Figure 15: Cross-section of the used micromembranes.

Site-selective depositions of different nanowire meshes of SnO_2, WO_3 and Ge to be used as vapour grown e-nose type sensor units were conducted. While Germanium exhibits excellent selectivity towards humidity, SnO_2 and WO_3 are sensitive to important gases like CO, NH_3 and NO_x.

3.1 Site-Selective Growth of SnO_2 nanowires

The deposition of SnO_2 nanowires from $Sn(O^tBu)_4$ precursor in a low pressure CVD reactor requires high temperatures of > 700 °C.[68] The benefit of this growth is the thermal initiation of the oxide formation while deposition in locations of low temperature is avoided. The issue of substrate temperature is also important for the use of multifunctional substrates with temperature sensitive areas. Although rather high temperatures are needed to deposit SnO_2, the temperature range of operation must not be too high, because the sticking coefficient decreases with increasing temperature. At high temperatures the adsorbed reactive species desorbs again instead of nucleating and no film is deposited as illustrated in Figure 16. In addition, in low pressure processes and very low oxygen partial pressure, the reduction of SnO_2 in SnO, which is more volatile, has to be considered to contribute to this process.

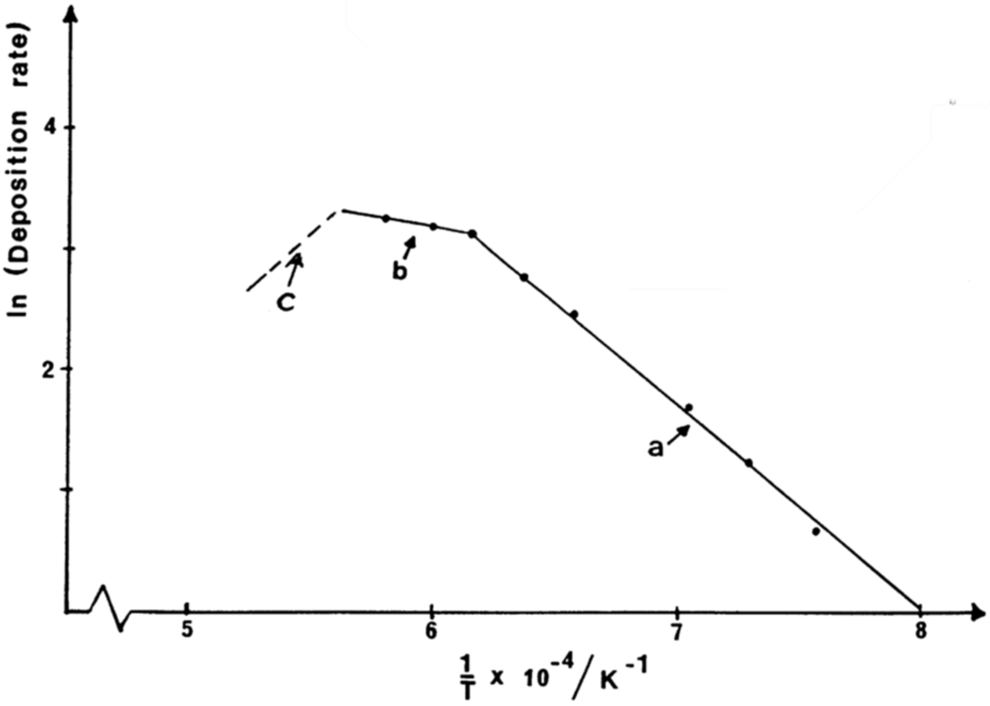

Figure 16: Exemplary diagram of the temperature dependant deposition rate of TiB_2 coatings. At region c, the CVD process is limited by the involved kinetics of the chemical reactions. At higher temperatures, region b, the increase of the deposition rate flattens, because the process is now mainly limited by the mass transport of the precursor. However, at even higher temperatures, region c, desorption causes a decrease of the deposition rate.[36] *Reprinted with permission from Elsevier.*

Investigations on the SnO_2 deposition without gold growth promoters shows the evolution of the deposit upon increase of temperature using $Sn(^tOBu)_4$ as precursor in a LPCVD setup. At lower temperatures, the deposition covers the whole heated area of the membrane as illustrated in Figure 17a. The temperature gradient in the used microhotplates causes the desorption in the middle of the membrane, where the temperature is too high. SnO_2 is still deposited at the outer regimes where the temperature is lower as shown in the SEM images in Figure 17c.

The SnO_2 nanowires grow via a VLS mechanism and therefore a thin gold layer was sputtered onto the micromembrane. The SnO_2 nanowires grow at high temperatures, reaching the thermomechanical limits of the micromembranes, especially at reduced pressure. Therefore, the micromembranes require careful heating and cooling cycles and extensive mechanical stress should be avoided. Temperature drops and very high precursor flux should be avoided in the SnO_2 nanowire growth process, because thin film deposition can interfere with the nanowire nucleation. The precursor flux should be controlled during the deposition in order to ensure reliable nanowire growth. The temperature of the precursor proved to be of significant importance as no deposition at all was observed at 24 °C, but at 26 °C nanowires were deposited.

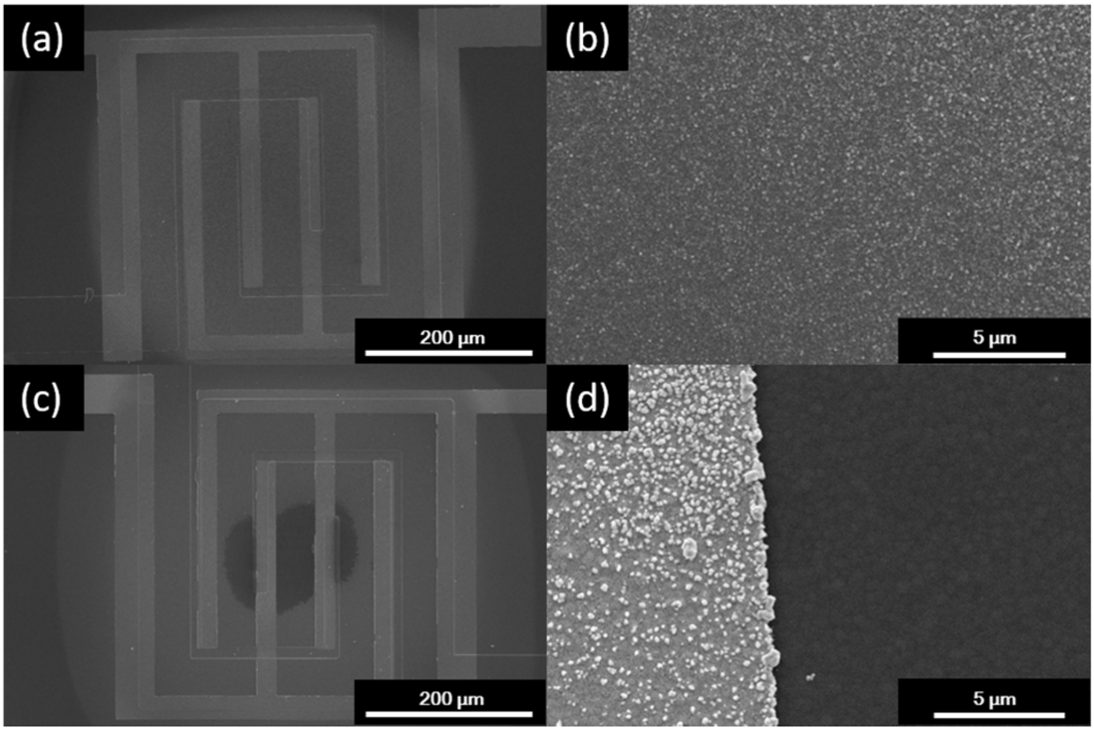

Figure 17: (a) Homogenous SnO_2 film is deposited at lower temperatures. (b) Higher magnification of the deposited film. (c) Higher temperatures cause a larger diameter of the deposited film, however, the high temperatures in the middle of the micromembrane cause desorption of the adsorbed reactive species and no deposition is observed. (d) Higher magnification provides evidence, that no film is deposited on the membrane but on the electrode.

Besides the precursor temperature und thus the flux, the deposition temperature required optimisation. There are two ways to control the temperature of the microhotplates, either by applying a constant voltage or a constant current. Applying a constant current has the advantage, that small changes in the pressure of the system are visible by a change of the resulting voltage. This method to control the pressure is very sensible and thus the opening of the valve can be controlled not to be too fast. However, the temperature cannot be precisely adjusted with the available equipment due to the step size of ±0.1 mA with the used source meter. Another drawback is the drop of temperature when the pressure increases which is inevitable when opening the valve of the precursor. On the other hand, when a constant voltage is applied the temperature can be better controlled, as the voltage can be changed by ±0.001 V. However, there is no indication of a change of pressure and one has to trust the pressure reading. In this study a constant voltage is used to control the process. The optimum deposition temperature is actually a quite small interval. A high temperature is needed to obtain a deposition area big enough to completely cover the sensing area of the micromembrane. Applying few millivolts more, the micromembranes tend to exhibit mechanical failure. In addition, unwanted morphologies such as nanobelts (Figure 18) are obtained at higher temperatures and the homogeneous nanowire deposition is targeted.

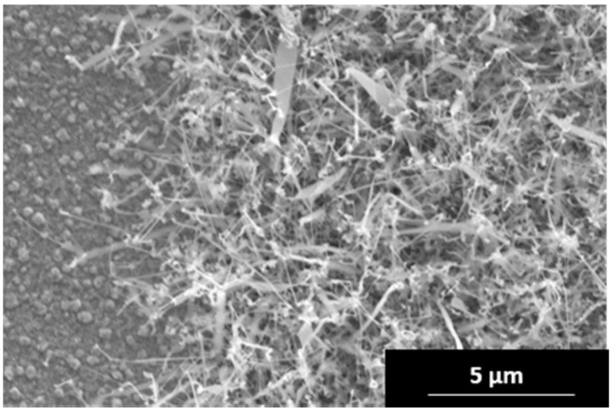

Figure 18: SnO_2 nanobelts were grown because of high deposition temperature and limited growth seed material, which could be caused by a high precursor flux at the initial nucleation stage.

By optimising the applied voltage, good quality nanowires could be grown. It should be noted however, that the process is strongly influenced from the other deposition parameters as well, of which the precursor flux is the hardest to adjust, because it is dependent on the amount of precursor and its temperature, the pressure of the evacuated LPCVD setup and how slow the valve is opened. Adjusting all the parameters, nanowires as shown in Figure 19 are obtained while higher temperatures lead to thinner nanowire deposits.

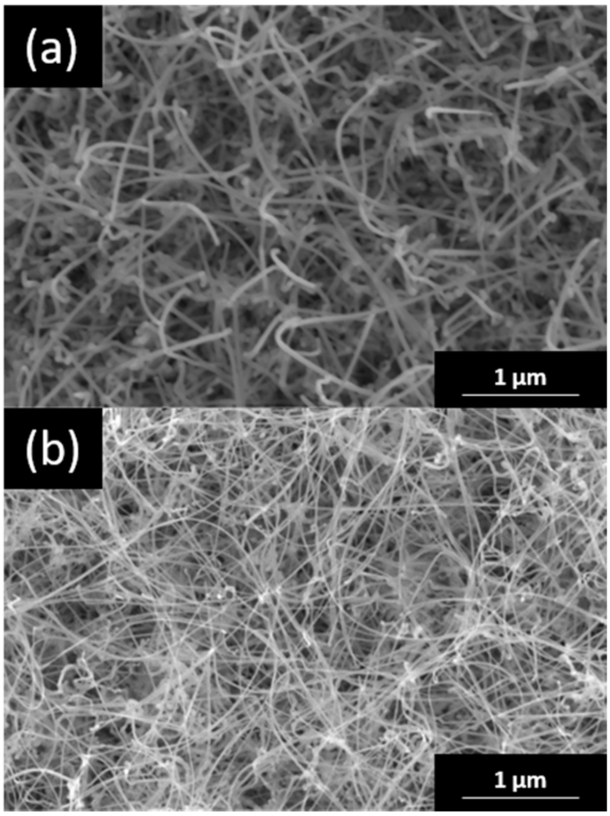

Figure 19: (a) To obtain SnO_2 nanowires of good quality not only the temperature has to be well adjusted, but also the precursor flux has to be taken care of. (b) At higher temperatures thinner nanowires are obtained.

The good quality of the as grown nanowires was also demonstrated by HRTEM as shown in Figure 20. The diffraction pattern reveals the growth in <101> direction.

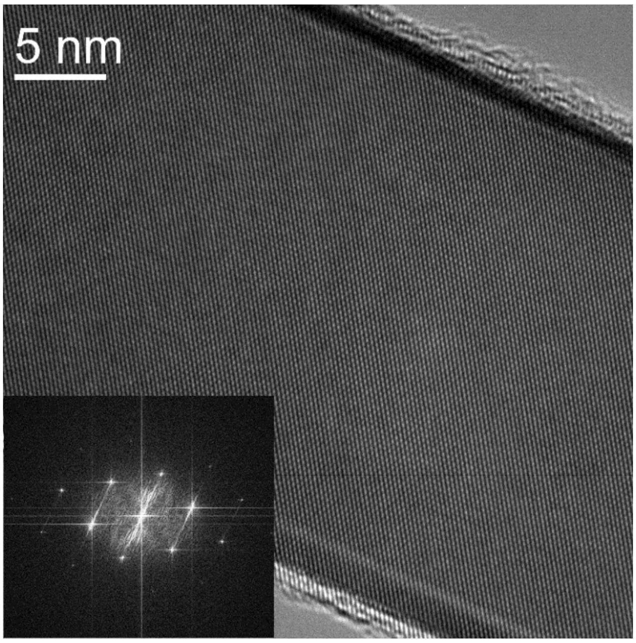

Figure 20: HRTEM image of a tin(IV)oxide nanowire grown in <101> direction, as proven by the diffraction pattern.

3.2 Site-Selective Growth of Ge nanowires

Germanium nanowires were grown using diphenylgermane as precursor in a LPCVD setup using a thin gold layer on the micromembrane as nucleation layer.

Germanium nanowires were already grown site-selectively on microhotplates,[10] but in order to optimise the process for micromembranes, different series of experiments have been performed. First, the appropriate voltage to heat the micromembrane to the ideal deposition temperature has to be determined. At temperatures too low, the precursor is not decomposed, while at temperatures too high an amorphous germanium film is deposited. Different precursor fluxes were investigated by varying the amount of diphenylgermane. The process varied significantly with the precursor flux. Figure 21 illustrates that the increasing amount of diphenylgermane leads to an increased precursor concentration in the gas phase, which results in a higher density of nanowires and length due to the increased deposition rate.

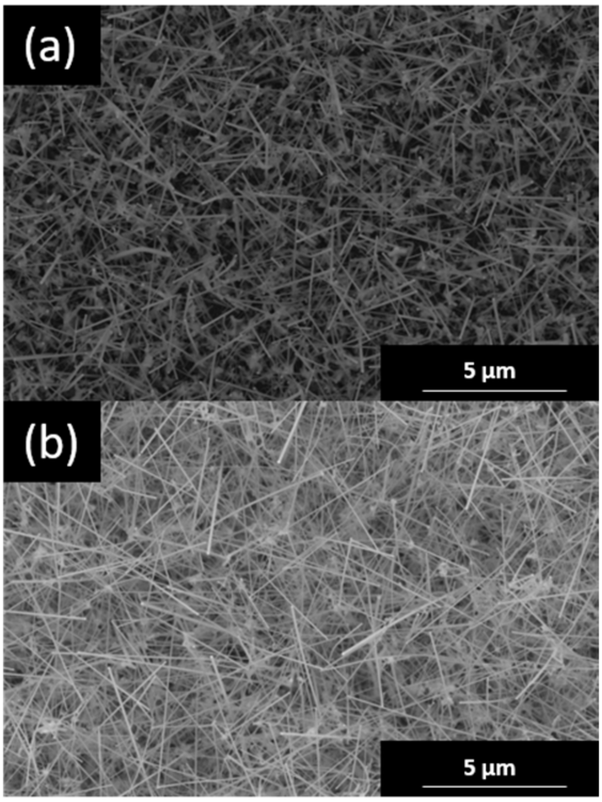

Figure 21: Germanium nanowires grown at 3.75 V for 10 min. More and longer nanowires are obtained when a threefold amount (b) of diphenylgermane was used when compared to (a).

The deposition was stopped after few minutes to investigate the nucleat ion stage. Germanium nanowires tend to grow along the surface and gold is accumulated leading to increasing nanowire diameter. This growth mode has to be avoided due to the formation of a highly conducting surface nanowire layer with low surface area connecting the electrodes. In order to optimise the nucleation and uplift the lying nanowires, the micromembranes were heated to a higher temperature during the first ten seconds of deposition to enhance the nucleation stage. This strategy of nucleation and growth regime was successfully used for the growth of perpendicular Ge nanowires using germane precursor.[106] However, these experiments did not lead to the targeted effect. The micromembranes with the two temperature procedure show reduced nanowire growth in in the middle of the heated area with the highest temperature (Figure 22). Normally, this would suggest, that the process is already in the desorption controlled deposition regime and that might be for the first ten seconds, but as the temperature is decreased afterwards, germanium nanowires should be deposited in the middle as well. Another hypothesis would be the deposition of an amorphous germanium film or carbon contamination leading to a deactivation of the gold growth seeds and thus inhibiting VLS growth.

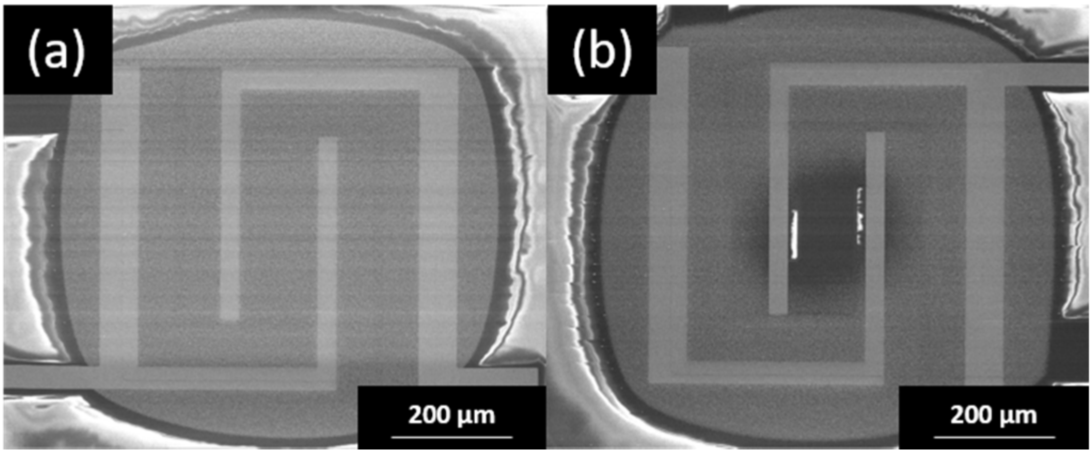

Figure 22: (a) Germanium nanowires grown on a micromembrane at 3.9 V for 10 min. (b) If the microhotplate is heated during the first ten seconds of deposition (4.3 V), no nanowires are deposited in the middle.

Optimised growth temperatures lead to a dense network of nanowires with low tendency of kinking and low numbers of nanowires growing along the nanowire surface. Figure 23 shows the undesired nucleation at lower temperature with highly kinked nanowires and also the growth of Ge nanowires along the surface at higher temperature. As the density is lower at higher temperatures, desorption of the active species probably already occurs.

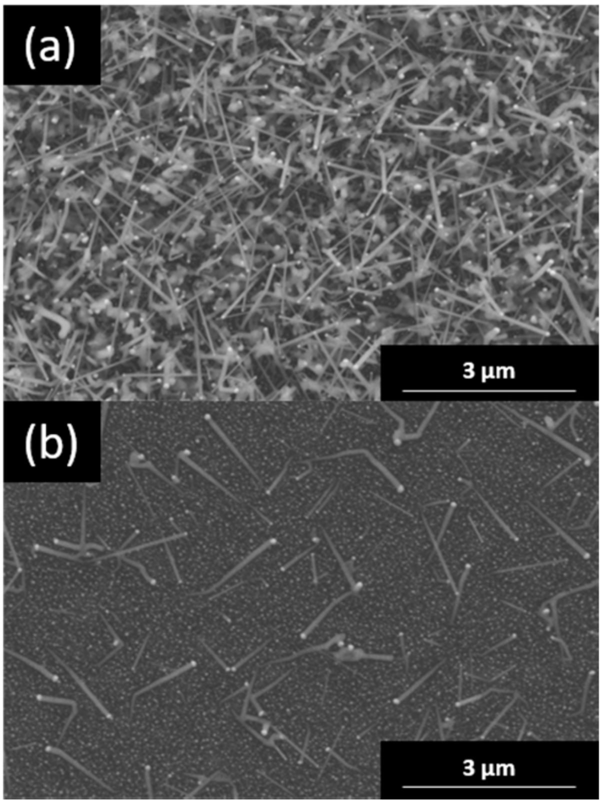

Figure 23: The deposition of germanium nanowires was stopped after 3 min to investigate the nucleation behaviour. (a) At low temperatures, nanostructures with many kinks nearly cover the whole surface, creating a conductive layer. (b) At higher temperatures, Ge nanowires grow along the surface with increasing diameter, because the seed gather gold from the surface. Both nucleation regimes have to be prevented and an in-between temperature was used.

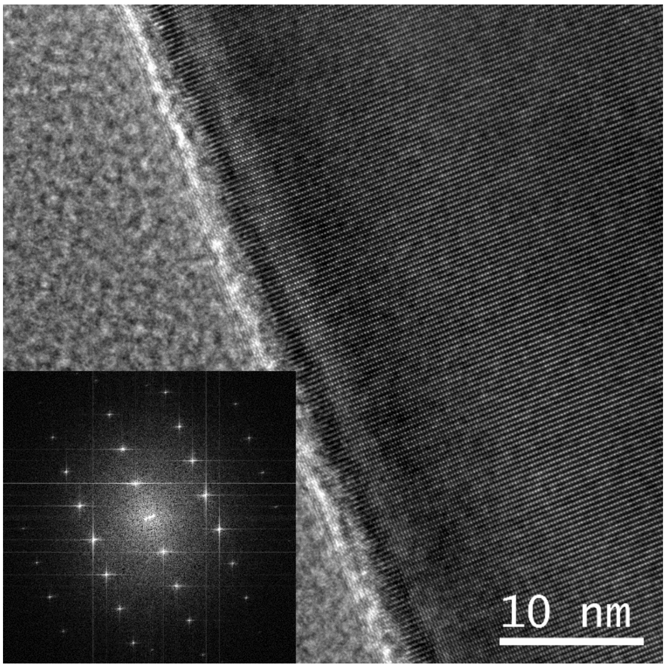

Figure 24: HRTEM image of a germanium nanowire grown in <111> direction, as proven by the diffraction pattern. A thin (ca. 1 nm) GeO$_x$ layer is visible at the edge.

HRTEM showed, that these Ge nanowires are coated with a thin, amorphous GeO$_x$ layer, that can be seen in Figure 24. The diffraction pattern reveals the <111> growth direction of the nanowires. The oxidised surface of the germanium nanowires seems to be critical for the sensing mechanism. The germanium nanowires were heated for 48 h under synthetic air in order to investigate the

stability, and stabilisation of response is achieved, when operating below 100 °C. At these moderate temperatures the predominant adsorbed oxygen species is O_2^- (5).

$$O_{2(g)} + * \rightleftharpoons O_{2(ads)}^{-} + h^{+} \tag{5}$$

Germanium nanowires respond to NO_2 (6), which causes a decrease of resistance, because the grown germanium is a p-type semiconductor. However, the oxidised surface forming a Ge/GeO$_x$ core-shell structure has to be considered in the sensing.

$$NO_{2(g)} + * \rightleftharpoons NO_{2(ads)}^{-} + h^{+} \tag{6}$$

Furthermore, the Ge nanowire networks respond to changes in the CO concentration (7). The response is strongly decreased when measuring under nitrogen atmosphere instead of synthetic air, suggesting that the mechanism is dependent on ionosorbed oxygen.

$$2CO_{(g)} + O_{2(ads)}^{-} + h^{+} \rightleftharpoons 2CO_{2(g)} + * \tag{7}$$

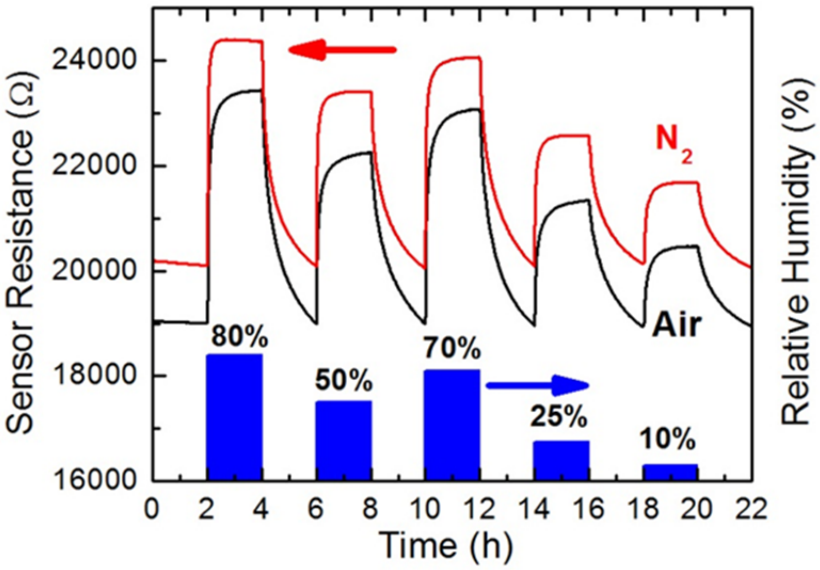

Figure 25: Response of the germanium nanowire sensor to water diluted in nitrogen (red) and synthetic air (black). Although there is an offset of the resistance, the response is the same, indicating the independence of the sensing mechanism on oxygen.[91]Reprinted with permission from Elsevier.

For metal oxide sensors the response to water vapour is normally attributed to a surface reaction with ionosorbed oxygen leading to chemisorbed hydroxy groups. However, investigations showed, that the response of the grown Ge nanowires to humidity is independent on the oxygen partial pressure as shown in Figure 25. The presence of oxygen only causes an offset of the measured resistance. This indicates, that at the relative low temperature of 100 °C water does not react with chemisorbed oxygen, but is chemisorbed itself.[91] On n-type silicon layers similar water adsorption induced a downward band bending, confirmed with Hall measurements.[107] The increasing resistance of the p-type germanium nanowires can be explained either by a charge transfer from the chemisorbed water molecules, or by a field effect caused by the dipole of water.

3.3 WO_3 nanowires in a cold wall CVD oven

According to literature, WO_{3-x} nanowires can be obtained with an AACVD setup by using $W(CO)_6$ as a precursor and methanol as oxidising agent as well as solvent in a hot wall reactor. However, in order to gain knowledge that is useful for site-selective growth of WO_{3-x} nanowires on micromembranes, a cold wall reactor was used. The used AACVD setup is shown in Figure 26. The precursor solution is placed in a two-necked flask and the carrier gas is bubbled through the solution while the gas flow was controlled with a MFC. An ultrasonic generator is used to generate the aerosol in the flask. The created aerosol is transported through the glass reactor to an inductively heated graphite susceptor as deposition zone. The temperature of the graphite susceptor is measured and controlled with a thermocouple. The susceptor is placed on a quartz boat to enable a better gas flow and prevent direct heating of the reactor walls.

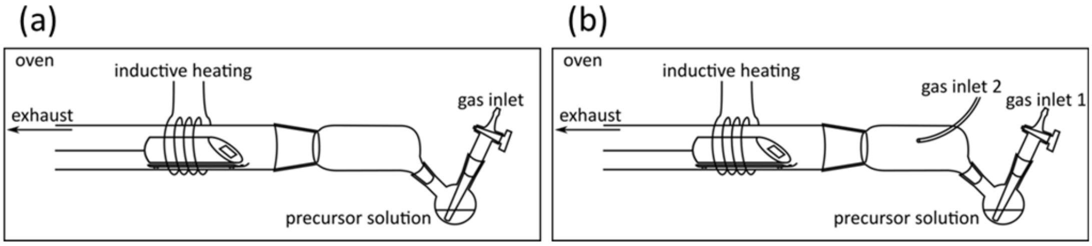

Figure 26: (a) AACVD setup that lead to premature deposition while heating up. (b) AACVD setup with an additional gas inlet to add a reactive gas or purge the reactor with an inert gas without bubbling through the precursor solution.

In principle, the growth of WO_{3-x} nanowires should be better controllable by using an inert solvent and adding oxygen to the carrier gas. First experiments using hexane as an inert solvent and compressed air as reactive gas have been unsuccessful to form tungsten oxide nanowires, probably because the VS growth mechanism is induced by the anisotropic crystal structure of some suboxides such as $WO_{2.77}$.[84] Therefore, if the O_2 partial pressure is too high, only fully oxidised WO_3 is obtained, and instead of nanowires a dense film is deposited. As a consequence, nitrogen has been used as carrier gas with traces of compressed air, using a modified setup with an additional gas inlet (Figure 26b). However, even at the lower limit of the available MFC, fully oxidised WO_3 is obtained as a film, that morphology was strongly dependent on the oxygen concentration (Figure 27a and b). Nevertheless, nanowire growth should be possible if using a more sophisticated gas mixing system to precisely control the oxygen amount.

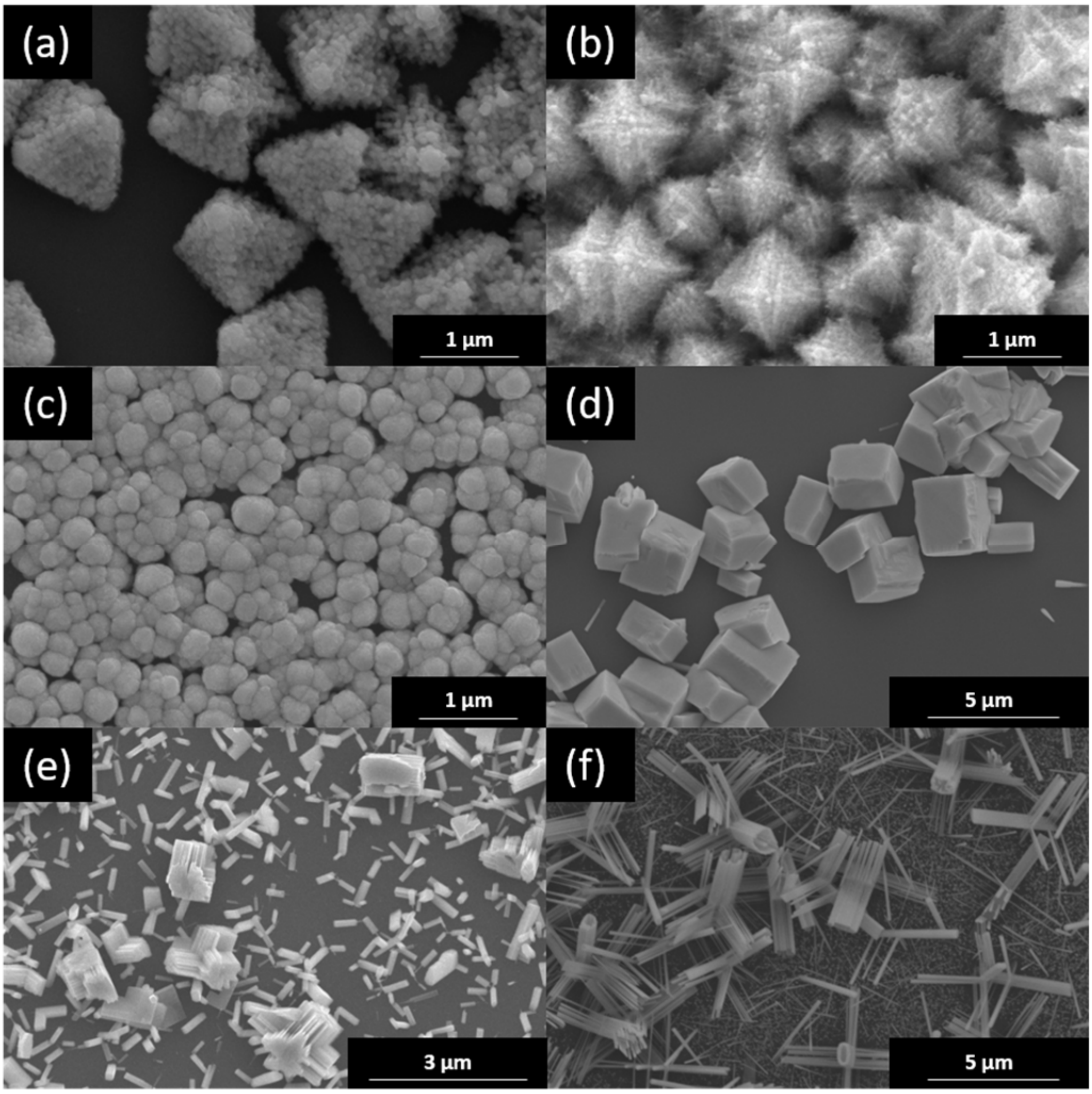

Figure 27: (a) WO_3 morphology obtained at 440 °C using hexane as an inert solvent and synthetic air as carrier gas (100 sccm) and oxidising agent. (b) WO_3 morphology obtained at the same temperature as (a), but nitrogen was used as carrier gas (100 sccm), while 10 sccm of synthetic air were added into the reaction chamber. To grow WO_{3-x} nanowires, the O_2 partial pressure probably has to be reduced even further. (c) First experiments with methanol as solvent and oxidising agent lead to a dense film of WO_3. (d) Reducing the concentration obtains angular microcrystals with few elongated structures in between. (e) By optimising the AACVD setup, by adding an additional gas inlet, nanorods between agglomerated multipods are obtained. (f) By reducing the gas flow and thus the precursor concentration in the reaction chamber, a mixture of nanotubes and nanowires is obtained.

Tungsten oxide nanowires are obtained by using nitrogen as an inert carrier gas and methanol as solvent as described in literature.[80] The gas flow and the concentration of the precursor solution have been adjusted and optimised in order to control the nanowire formation (Figure 27c-f). This adjustment is necessary, because the growth is carried out in a cold wall reactor instead of the hot wall CVD setup described in literature. The cold wall reactor setup is used to obtain comparable parameters for site-selective deposition on micromembranes mounted to a TO-8 package.

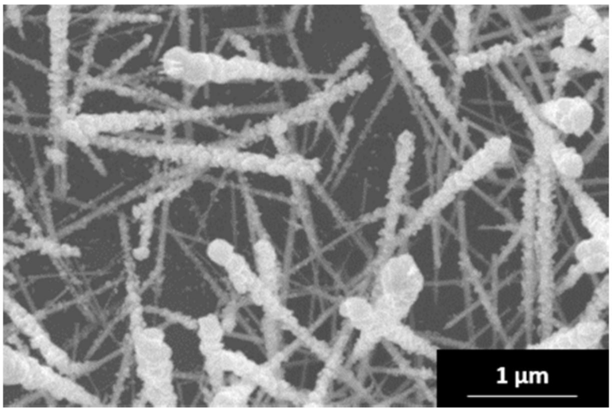

Figure 28: Nanowires grown at 360 °C with methanol as solvent and oxidising agent and nitrogen as carrier gas (60 sccm). The undesired secondary deposition at the nanowire has to be avoided to take full advantage of the high crystallinity of the deposit, which requires further optimisation.

In the first setup (Figure 26a), nitrogen is bubbled trough the precursor solution while heating up the susceptor to purge the reactor. In this stage a premature deposition is obtained, which can be caused by the high volatility of methanol and $W(CO)_6$. Although nanowires are formed, unwanted secondary deposition is observed on the nanowires (Figure 28). This suggested, that nanowires are obtained by very low precursor concentrations in the gas phase. However, premature deposition at lower temperatures has to be prevented and therefore the setup (Figure 26b) has been modified adding a second gas inlet to the reaction chamber. Thus, the reactor can be flooded and purged with inert gas without carrying precursor to the substrate. Initial experiments with this setup show the formation of predominantly multipods (Figure 29) with only few individual nanowires.

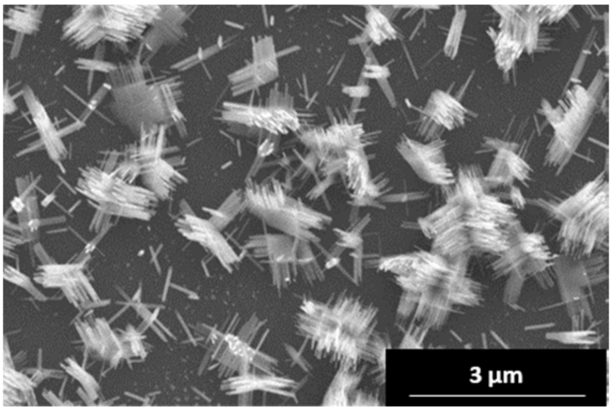

Figure 29: Occasional WO_{3-x} nanowires between WO_{3-x} multipods, obtained at 350 °C. Methanol was used as solvent and oxidising agent and nitrogen as carrier gas (60 sccm).

Differences in the hot wall and cold wall CVD experiments and the influence on the reacting species have been considered. In a hot wall reactor, the alcohol and tungsten carbonyl can react to form alcoholate intermediates or alcohol adducts prior to the decomposition of the precursor on the heated surface. Therefore, the reaction of the $W(CO)_6$ with methanol has to be considered.

Ultrasonic treatment $W(CO)_6$ in methanol does not lead to any changes of the infrared (IR) spectra of the carbonyl; however, ultraviolet (UV) light triggers the conversion to alkoxo-carbonyl-tungsten compounds. A change in colour is observed in precursor solutions already hints towards a reaction of the starting compounds upon exposure to ambient light, while the same solutions remains colourless in the same solution when kept in the dark. The FTIR-spectra for the ultrasonically treated sample and the mixture from the unexposed solution remain unaltered, while the UV-light exposed solution shows least two more carbonyl absorption bands (Figure 30). This already hints towards an exchange with methanol and possible preoxidation to an alkoxide species, which is in agreement with literature.[108] Monosubstitution of $W(CO)_6$ would reduce the symmetry from O_h to C_{4v}, resulting in three IR active carbonyl absorption bands instead of one.[109] Only two additional absorption bands are observed, either because the signal-to-noise ratio is not sufficient, or two absorption bands have wave numbers too similar to be distinguished.

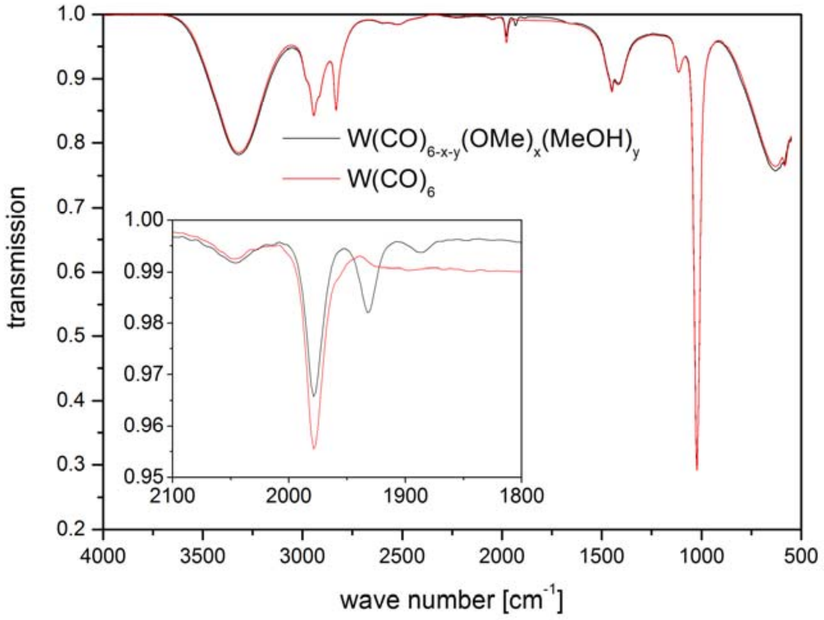

Figure 30: FTIR spectra of preoxidised precursor solution (black) and freshly prepared solution of W(CO)₆ (red). In the carbonyl regime at least two more absorption bands are visible, indicating a light induced ligand exchange.

After discovering the necessity of a light induced ligand exchange, the precursor solution has been exposed to light for an hour before the deposition and the concentration. The precursor solution has been optimised, leading to the desired site-selective deposition of WO_{3-x} nanowires without multipods or secondary depositions as shown in Figure 31.

Ageing of the precursor solution is necessary to grow individual nanowires meshes without multipod formation and secondary deposition on the nanowires as shown in Figure 31. XRD investigations point towards the $W_{18}O_{49}$ phase (Figure 32), but due to the anisotropic growth only few reflexes are observed and indication of the structure to a specific phase is difficult.

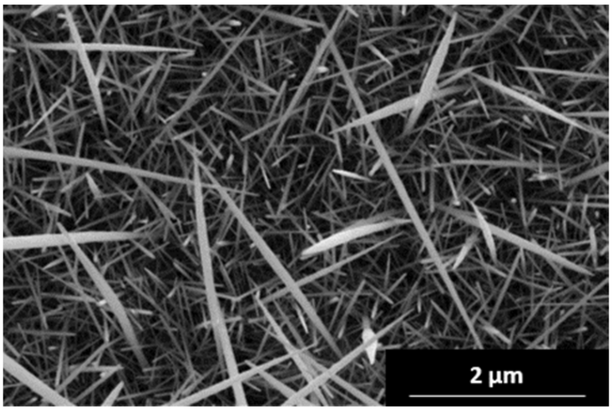

Figure 31: WO_{3-x} nanowires grown on a silicon substrate at 360 °C. Methanol was used as solvent and oxidising agent and nitrogen as carrier gas (50 sccm). The solution was aged to preoxidise the precursor.

As the WO_{3-x} nanowires are designed to be used as gas sensor material and thus should operate under ambient conditions at high temperatures, their stability has been proven by SEM and XRD investigations after heating to 400 °C for few hours at air. Although at these conditions the material is fully oxidised, the nanowire morphology is preserved. XRD investigations show a shift to smaller angles of the measured reflexes, as the unit cell grows with more incorporated oxygen and the positions of the reflexes are in correspondence with the reference data for WO_3 [PDF 01-083-0950].

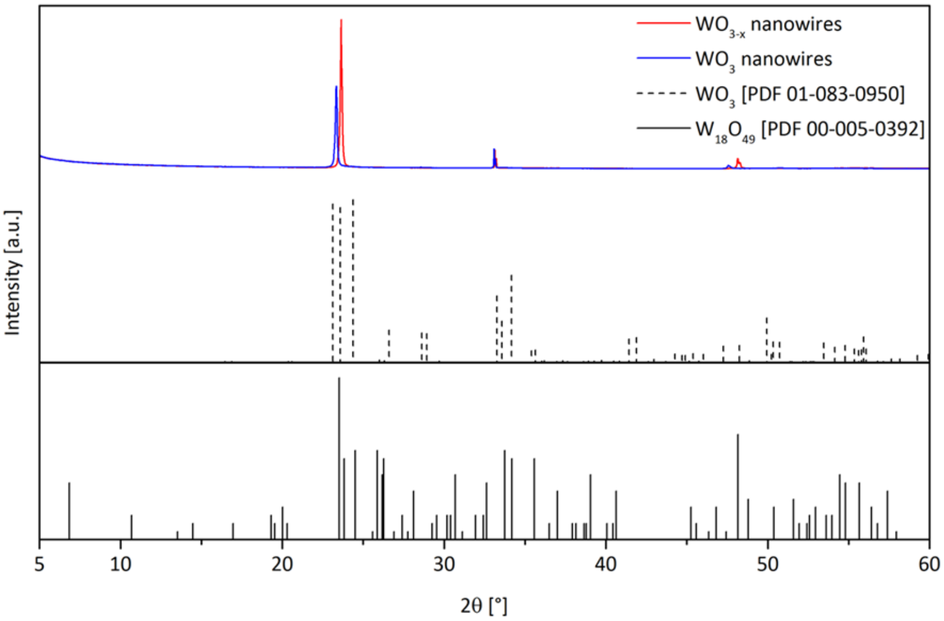

Figure 32: XRD of WO_{3-x} nanowires (red) grown on a silicon substrate. After oxidation, the elongated morphology is obtained (blue), a shift to smaller angles indicates the growth of the unit cell after incorporation of more oxygen. Due to the elongated growth, only few reflexes are observable, complicating the identification of the crystal structure. References of WO_3 and $W_{18}O_{49}$ are added for comparison as possible candidates. The reflexes at 33.0° are relatable to unknown contaminations in the substrate.

3.4 Site-Selective Growth of WO_3 nanowires

After optimisation of WO_{3-x} morphology in a cold wall AACVD setup, site-selective growth has been targeted. An AACVD reactor similar to the one used in the cold wall oven has been designed to accommodate the electrical contacts to connect the TO-8 package. Although the new setup is very similar to the graphite susceptor containing assembly, the flow needs to be adjusted to obtain the optimal growth conditions. The key to success was to accelerate the aerosol with a second flow of nitrogen, using a setup similar to Figure 26b.

The optimal deposition temperature in the cold wall reactor is 360 °C in good agreement with literature. First experiments with the micromembranes have not resulted in the growth of nanowires even though the nominal temperatures of the calibrated micromembranes have been used. Higher voltages and thus higher heating power result in the successful growth in nanowires. In the literature this is described as a temperature offset compared to conventional CVD[79] but probably the temperature is only seemingly higher, since temperature calibration of the micromembranes has been performed in air and it seems that the aerosol flow and evaporation of the solvent has a strong cooling effect. To precisely control the local temperature at the surface of the micromembrane a pyrometer would be desirable to measure the temperature under growth conditions.

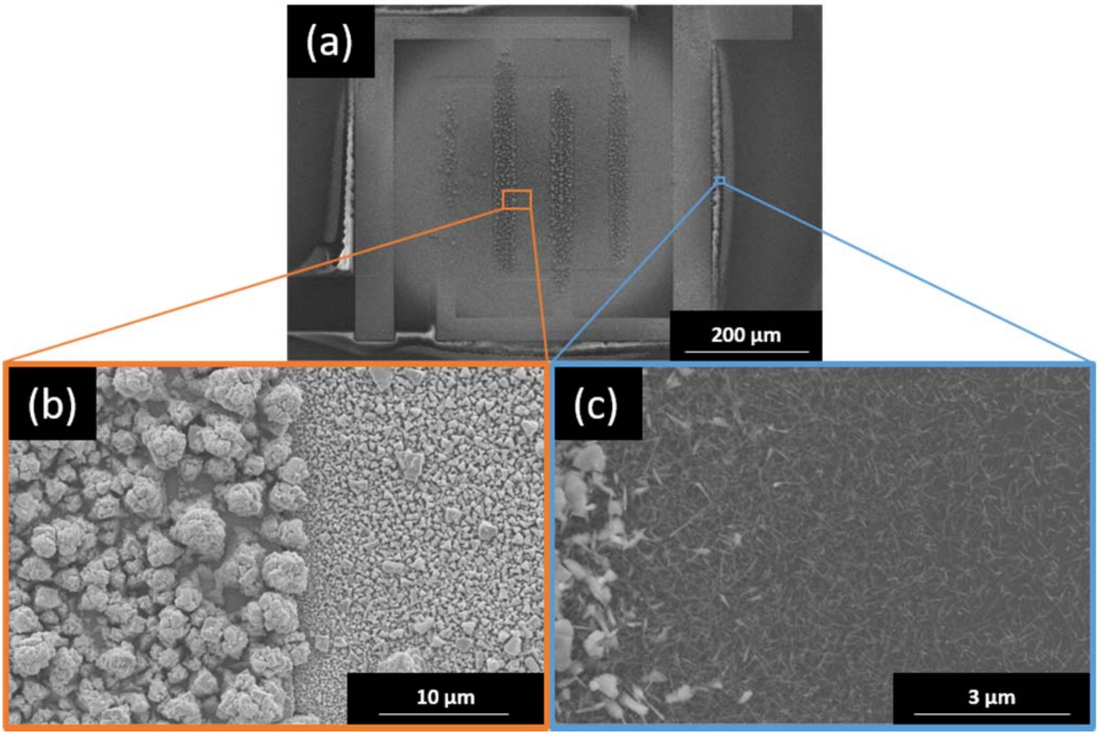

Figure 33: (a) WO_{3-x} deposited on a micromembrane at temperatures too high. (b) Higher magnification of they morphology deposited at too high temperatures in the middle of the membrane. (c) Higher magnification of the outer right electrode, where due to the temperature gradient nanowires were deposited at lower temperatures.

A series of experiments with the same aerosol flow yield nanowires at high voltages in the periphery of the micromembrane for the highest temperatures. The temperature profile of the micromembranes includes a tailing where the resistive heater is not located, which is the outer region of the micromembrane. The used voltage has caused a temperature that is a nuance too high in the middle since the nanowires are located just outside of the interdigitates (Figure 33).

After finding the optimal temperature, the gas flow had to be optimised. As already mentioned, there are in fact two gas flows to optimise, the one bubbling through the solution and the second, of the gas inlet to the reaction chamber, which was used to accelerate the aerosol. The same results are obtained for intentionally aged precursor solutions and also solutions used twice in a sequence of depositions. Individual nanowires are only obtained, when the precursor solution is used for a second deposition on the same TO-8 chip, while at the first deposition contains multipods with quasi-aligned nanowires (Figure 34).

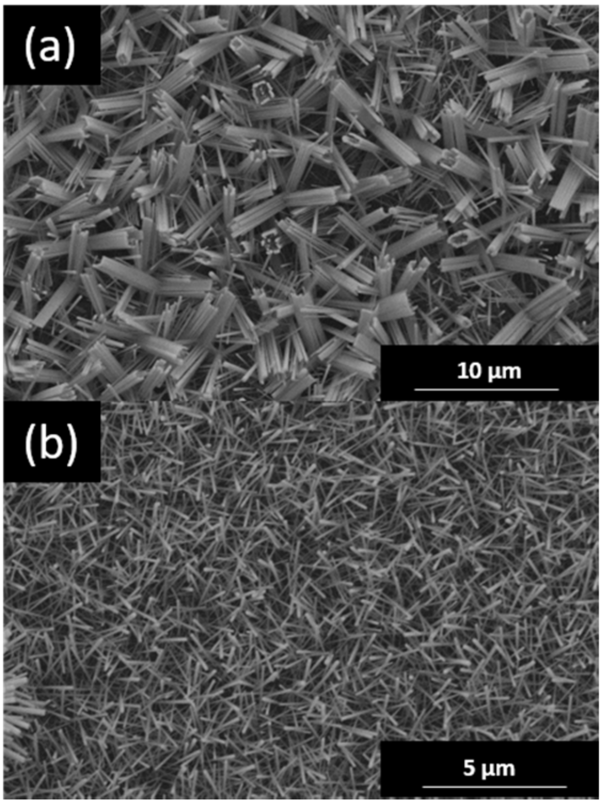

Figure 34: (a) WO_{3-x} nanostructures site-selectively grown on micromembranes. Although completely different morphologies are obtained, the only difference between (a) and (b) is an ageing of the precursor solution.

The precursor solution has been aged and the concentration of the precursor has been optimised for the deposition on the micromembranes. This leads to the desired site-selective deposition of WO_{3-x} nanowires without multipods as shown in Figure 35. Additional nucleation of a particle deposit in the early stages of deposition has to be avoided, because the undesired secondary deposition may form a conductive layer interfering with the targeted tungsten oxide nanowire mesh (Figure 35a). The initial stage of the deposition is crucial, because the nanowire growth seeds are formed and these initial crystals lead to nanowire formation. By precisely controlling the temperature in the beginning of the CVD process, such secondary depositions are inhibited, as shown in Figure 35b.

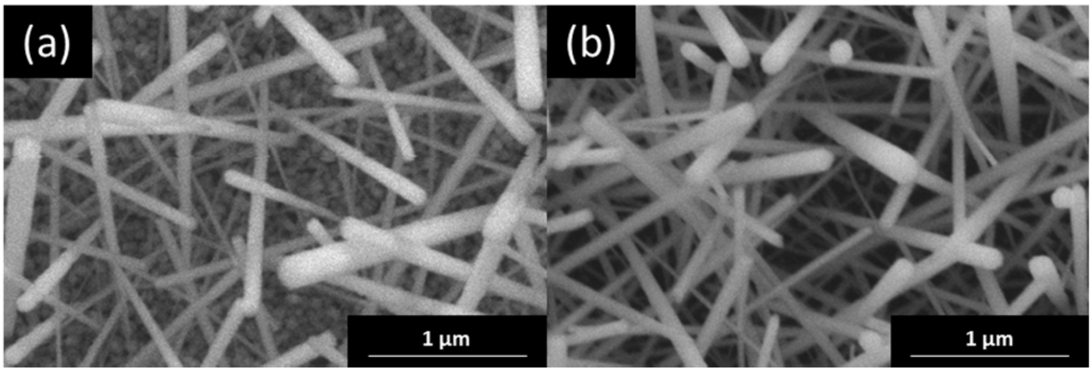

Figure 35: WO_{3-x} nanowires grown site-selectively on a micromembrane. By optimising the process parameters undesired deposition (a) in the area of the interdigitates is avoided (b).

The network of WO_{3-x} nanowires does not spread over the whole micromembrane and does usually not connect the outer electrodes (Figure 36). Nevertheless, by connecting the inner two electrodes gas sensing can be performed as long as no conductive layer is connecting the other electrodes, which is not the case. To completely cover the sensing area, a higher temperature would be necessary, thus increasing the radius of the temperature that is high enough to grow nanowires. However, increasing the temperature too much, changes the morphology of the deposition. Therefore, to further improve the system, another design of the micromembranes would be necessary, in which the temperature gradient is smaller, or the distance of the outer electrodes is decreased. Furthermore, a transition zone is visible on the outside of the membrane with different morphologies. These structures cannot be prevented due to the temperature gradient of the microhotplate, but as they are outside of the sensing device, they do not affect the sensor performance, which will be tested in the future.

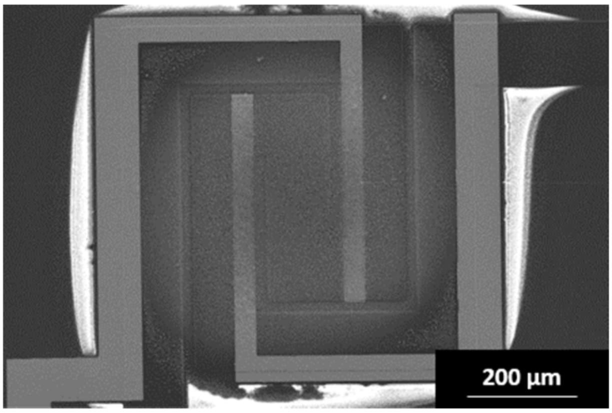

Figure 36: Transition zone of WO_{3-x} at lower temperatures at the edge of the micromembrane.

3.5 Site-selective Growth of WO_{3-x}, SnO_2 and Ge nanowires on one TO-8 package

The final stage towards an e-nose configuration is the deposition of the nanowires on different micromembranes of the same chip. Following the successful CVD growth processes for WO_{3-x}, SnO_2 and Ge nanowires, the subsequent deposition processes have been targeted. In principle, the order of deposition should be irrelevant, as the depositions only occur locally. However, precursor molecules can adsorb on the surface of the non-heated micromembranes and in fact affect other depositions and especially the desorption of tin oxide can alter the growth of the following materials.

Two of the four available micromembranes were coated with a thin Au film to enable SnO_2 and Ge nanowire growth. WO_{3-x} nanowires are grown via a VS mechanism and thus their formation is not dependant on a gold surface. However, after depositing SnO_2 nanowires, there seems to be an increased amount of nucleation seeds or a slight modification of the surface properties leading to more nucleation centres and a coating with tungsten oxide nanorods has been obtained in contrast to individual nanowires (Figure 37). For this reason, SnO_2 nanowires were deposited as a last step. This might be a small contribution of the material desorbing at higher temperature operation during the SnO_2 nanowire growth.

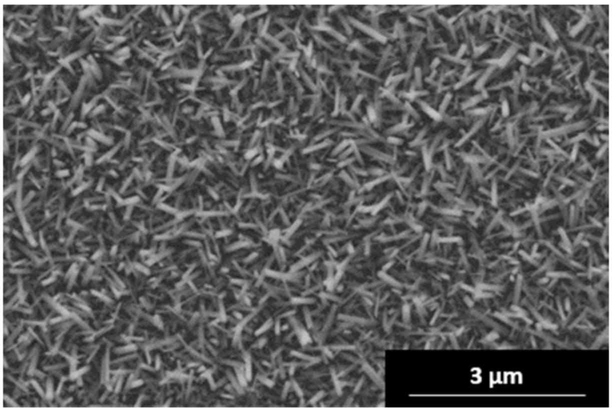

Figure 37: WO_{3-x} nanorods are grown after deposition of SnO_2 when applying the same process parameters that normally lead to nanowires. It seems that there are more nucleation seeds and therefore the density of the nanostructures increases, while the aspect-ration is decreased.

The nucleation of WO_{3-x} nanowires also was slightly influenced by the former deposition of germanium nanowires which results in higher nanowire density. Germanium is deposited first, followed by WO_{3-x} nanowires and finally the SnO_2 nanowires. A washing step with ethanol was implemented to avoid contamination with $W(CO)_6$ after the AACVD process. The ethanol has to be dried very slowly at air, because otherwise the network of nanowires shows the formation of closely attached nanowire bundles due to the high capillary forces of the evaporating ethanol, which decreases the surface-to-volume ratio as can be seen in Figure 38.

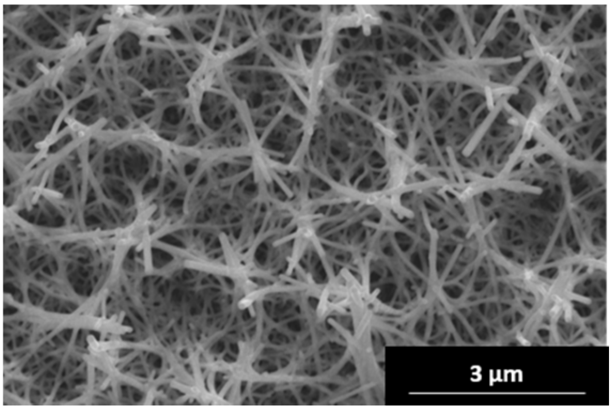

Figure 38: WO_{3-x} nanowires grown site-selectively after deposition of germanium nanowires on the same TO-8 package. Nanowire bundles can be observed after fast evaporation of ethanol due to capillary forces.

Finally, SnO_2 could be deposited after germanium and WO_{3-x} without any changes. As WO_{3-x} is the least selective gas-sensitive resistor of these materials, two micromembranes were functionalised with WO_{3-x} nanowires, so that the selectivity can be improved by measuring at two different temperatures. Figure 39 shows the final device with SEM images of the deposits in higher magnification. These chips are currently investigated for their gas sensing properties. The presented chip is the successful demonstration of a substrate containing three different site-selectively deposited and integrated nanowire materials for device operation.

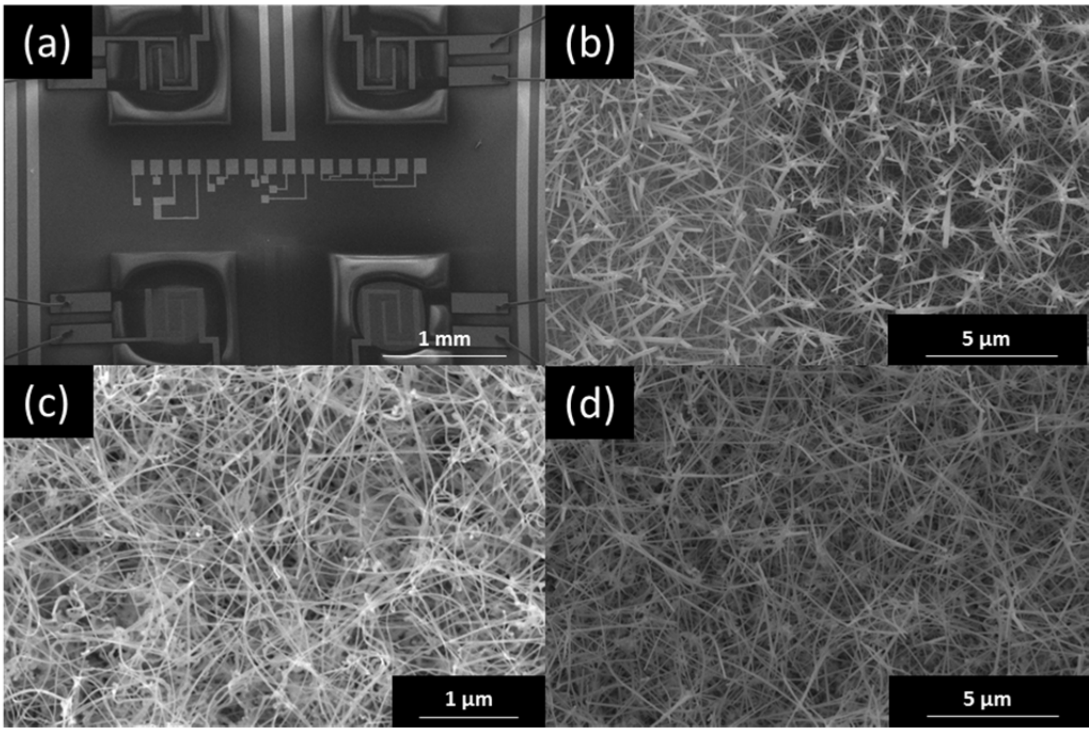

Figure 39: (a) Overview of the final device containing four micromembranes with WO_{3-x} nanowires (upper two), SnO_2 nanowires (lower left) and Ge nanowires (lower right). (b) Higher magnification of deposited WO_{3-x} nanowires. (c) Higher magnification of deposited SnO_2 nanowires. (d) Higher magnification of deposited Ge nanowires.

3.6 Modification of nanowires with MOFs

3.6.1 Conversion of ZnO to ZIF-8

The selectivity of the e-nose could be increased by using a filter material covering the nanowires enabling a pre-selection of analytes. MOFs should be a good candidate for this purpose and initial experiments for the formation of a MOF layer have been performed in this thesis. The initial experiments are based on ZnO nanowires which are grown on a seed layer of ZnO. The seed layer is deposited in the first step via spin-coating of an ethanolic zinc(II)acetate solution and following calcination. The ZnO nanowires are grown in an aqueous zinc(II)nitrate solution as reported in literature.[110] Polyethylenimine and hexamethylenetetramine are added to the growth solution as surfactant to support the formation of elongated crystals. While in the literature conversion of ZnO to ZIF-8 is mainly described by reactions in solution,[111-115] in this work the conversion was realised vie the gas phase by heating an evacuated flask containing 2-methylimidazole, the substrate with the ZnO nanowires and few drops of dimethylformamide. Figure 40 shows the obtained ZnO nanowires and the resulting core-shell structures after the conversion to ZIF-8. Figure 41 shows the XRD of the synthesised ZnO nanowires before and after conversion to ZIF-8.

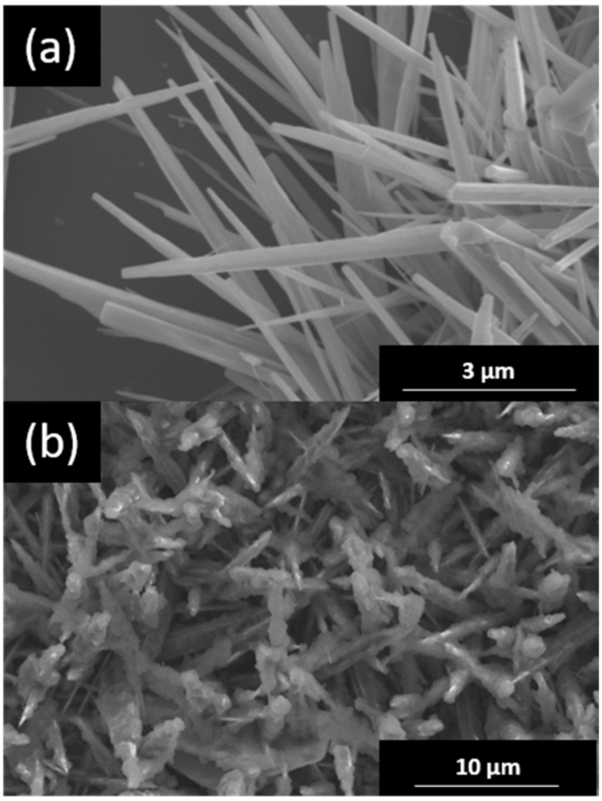

Figure 40: ZnO nanowires grown before (a) and after (b) conversion to ZIF-8. (b) Core-shell structures were obtained after 3 h.

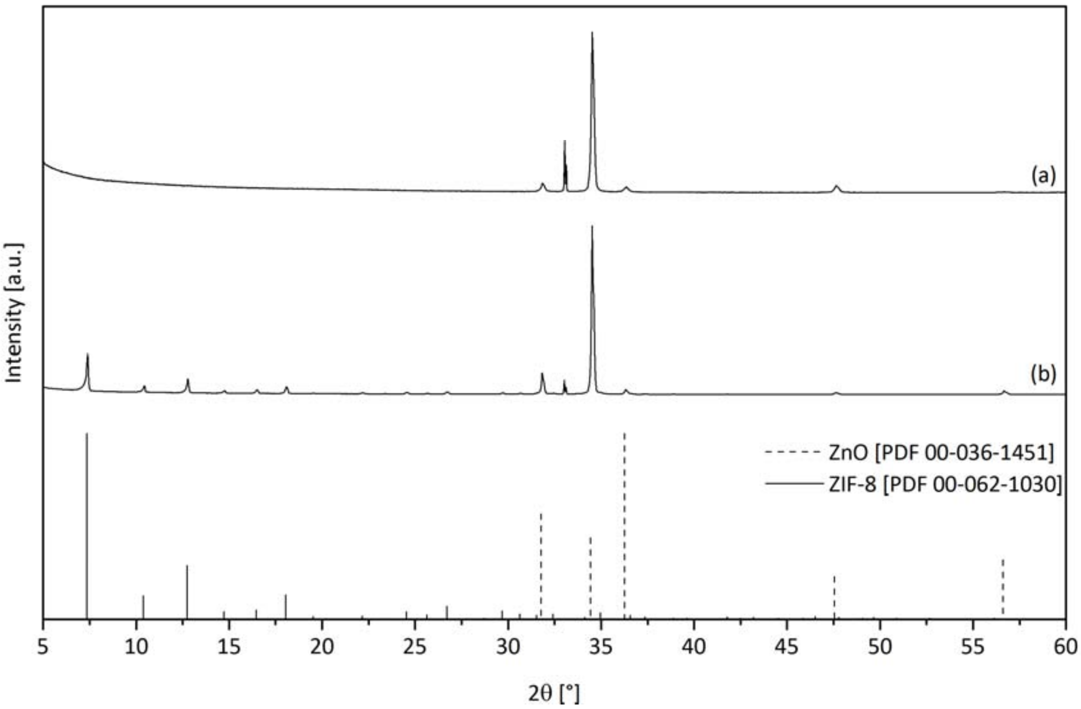

Figure 41: XRD of ZnO nanowires (a) and the obtained core-shell structure after conversion to ZIF-8 (b) grown on a silicon substrate. The reflexes at 33.0° can be related to inherent contaminations on the substrate. For comparison, two references are added. ZnO in dashed and ZIF-8 in solid lines.

The resulting core-shell structures could be used as gas-sensitive resistors, in which the MOF acts as a membrane. However, only single nanowires can be used for measurements, because there is no electrical contact between the nanowires due to the insulating MOF. Therefore, to use a network of nanowires as gas sensing layer, the nanowires have to contact each other, before a MOF is deposited around the mesh, which could be realised by a layer-by-layer growth.[56]

3.6.2 Construction of a layer-by-layer setup

A layer-by-layer setup is build/assembled to form a hybrid material consisting of a nanowire network surrounded by a MOF that acts as a membrane to improve the selectivity for gas sensing applications. The growth procedure requires subsequent dipping of a substrate in different solutions and this process requires an automatisation. For this purpose, a 4 degrees of freedom hobby robotic arm (Velleman KSR10) with DC motors is equipped with potentiometers and controlled with an Arduino microcontroller to create a robot able of closed loop motions as shown in Figure 42. A suitable program was written for the Arduino microcontroller that immerses an object held by the robotic arm subsequently into six different beakers. The duration of immersion in each beaker can be programmed individually as well as the amount of cycles. This is the base for a following surface-anchored growth of MOFs on nanowires in order to enable the formation of more sophisticated heterostructures for chemiresistor-type gas sensing applications.

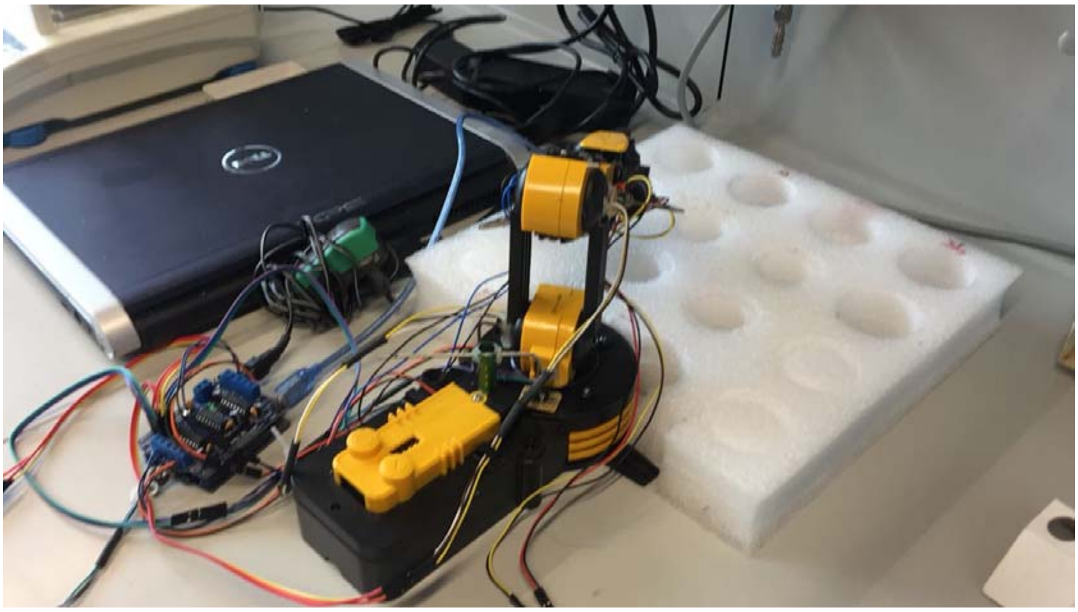

Figure 42: Self-made robot arm capable of closed loop motions. A hobby robotic arm has been equipped with potentiometers as feedback sensors. An Arduino Uno board equipped with a motor shield controls the robotic arm.

4 Summary

The morphology evolution of nanostructured WO_{3-x} obtained using an AACVD setup has been investigated. Nanowires with high aspect-ratio have been obtained by adjustment of the substrate temperature, the flow of the carrier gas and the concentration of the precursor solution. In addition to the process parameters, a pre-treatment of the precursor solution by aging under ambient light leads to modification of the tungsten carbonyl to $W(CO)_{6-x-y}(OMe)_x(MeOH)_y$. This modification is mandatory for an efficient growth of WO_{3-x} nanowire networks without secondary deposition of nanostructures on the membrane surface or the nanowires. The gained knowledge has been transferred to micro-CVD, where WO_{3-x} nanowires were grown site-selectively on a micromembrane. This is the first process leading exclusively to tungsten oxide nanowires on a small heated area. No additional deposition observed on the non-heated surface of the chips and the remaining hotplates can be used for deposition of other materials.

To create a useful device, SnO_2 and Ge have been chosen as additional gas sensing resistors. For this purpose, the LPCVD processes have been optimised in regard to deposition temperature, precursor temperature, pressure, and amount of precursor to ensure the best growth conditions on the available micromembranes. The reason for the absence of a SnO_2 layer has been attributed to a high temperature desorption process leading to the absence of this film. Finally, site-selective growth of all three different materials on one chip has been demonstrated for the first time. This technology enables the *in-situ* integration of nanowires in functional electronic devices like electronic noses, in contrast to other time consuming integration methods for nanowires.

The selectivity is still a problem for gas-sensitive resistors and the here demonstrated site-selective growth might be not sufficient enough for a targeted low power operation of devices. For this purpose, the modification of gas sensitive nanowires with an integrated membrane is demonstrated by converting ZnO to ZIF-8, creating a core-shell structure. This MOF may be used as a membrane to enable a selective sensing using the same sensor material and different MOFs. Furthermore, a setup to grow MOFs on nanowires via the layer-by-layer method has been assembled and will be the base for further investigations. The LBL method should enable the growth of various MOFs on all kind of nanowires and thus improve the selectivity of chemiresistors.

5 Experimental

5.1 WO_{3-x} nanowire growth procedure

WO_{3-x} nanowires are grown in a cold wall CVD oven as described of low pressure operation in literature. 50 mg of $W(CO)_6$ are dissolved in 15 ml methanol for the AACVD process used in this study. The solution was exposed to light for an hour, to preoxidise the precursor via a light-induced ligand exchange. An aerosol was generated with an ultrasonic humidifier and transported with 50 sccm of nitrogen to the reaction chamber. A silicon substrate was glued with conductive silver paint on a graphite susceptor, that was inductively heated to 360 °C. A light blue deposit was visible after 60 min of deposition.

To site-selectively grow WO_{3-x} nanowires on a micromembrane, 40 mg of $W(CO)_6$ are dissolved in 15 ml methanol in a two-neck flask that is attached onto a glass AACVD setup. 10 sccm of nitrogen are bubbled through the precursor solution to transport the aerosol and another 100 sccm of nitrogen are added into the reaction chamber to the second gas inlet to achieve an optimised deposition. A voltage of 6.2 V (7.2 mA) is applied to the microhotplate for the heating of the device. Although calibration of the micromembranes suggests a much higher temperature, approximately 360 °C are expected by comparison with cold wall experiments. Obviously, the aerosol flow has a strong cooling effect. After 60 min of deposition, the TO-8 packages were washed three times in ethanol to clean the surface of $W(CO)_6$. A blue deposit was visible on the micromembrane, surrounded by a white transition zone at lower temperatures.

5.2 SnO_2 nanowire growth procedure

SnO_2 nanowire growth requires approximately 10 mg of $Sn(^tOBu)_4$ in a dry flask. The vessel is evacuated to 10^{-2} mbar for 20 minutes in order to reduce the initial precursor gas pressure. Afterwards, the flask is attached to a glass LPCVD setup and a waterbath is used to ensure a constant 26 °C precursor temperature. Before heating the micromembranes, the whole setup is evacuated to 10^{-1} mbar. After cautiously applying 6.1 V (5.4-5.5 mA), the valve is opened very slowly. After 30 min, the deposition is stopped by closing the valve, slowly decreasing the voltage and carefully venting the setup. A white deposit is visible on the micromembrane.

5.3 Ge nanowire growth procedure

Ge nanowires are grown by adding ~15 mg of diphenylgermane with a cannula in a glove box into a flask, that was attached to a stainless steel LPCVD setup. The whole setup was evacuated to $2 \cdot 10^{-2}$ mbar. After applying 3.7 V (4.0-4.1 mA) the growth is initiated by opening the precursor valve. After 10 min, the deposition is stopped by closing the valve and reducing the voltage. A brown deposit of Ge nanowires is obtained on the micromembrane.

5.4 ZnO nanowire growth procedure and MOF modification

To grow ZnO nanowires on silicon substrates, a thin ZnO seed layer is produced by spin coating a 10 mM ethanolic zinc(II)acetate solution with 3000 rpm for 30 s. The thin film is dried on a hotplate for 15 min at 100 °C. This process is performed five times before the resulting film has been calcined at 350 °C. To grow ZnO nanowires on this seed layer, the substrates is placed in a 45° angle upside down in a solution containing 25 mM $Zn(NO_3)_2 \cdot 6H_2O$, 25 mM hexamethylenetetramine and 7 mM polyethylenimine (800 g/mol) in a snap cap vials. The assembly is heated to 90 °C in an oven. The solution is renewed three times per day and after two days the substrates are removed, washed with water and heated to 350 °C in a furnace. To further convert ZnO to ZIF-8 creating core-shell structures, the substrates are placed in Schlenk tubes, together with 0.4 g 2-methylimidazole and ten drops DMF. The Schlenk tubes are evacuated to increase the concentration of 2-methylimidazole in the gas phase and heated in an oven at 70 °C. After 3 h, core shell structures are obtained.

5.5 Characterisation

The XRD patterns were recorded on a PANalytical X-Pert PRO PW 3050/60 in Bragg–Brentano geometry and Cu-K_α radiation.

SEM analyses were performed on a FEI Quanta 200 scanning electron microscope.

TEM analyses were performed on a FEI TECNAI F20 transmission electron microscope operated at 200 kV.

FTIR investigation were conducted on a Bruker Tensor 27 with an ATR MicroFocusing MVP-QL with a diamond crystal using OPUS version 4.0 software for analysis.

6 Literature

[1] T. Seiyama, A. Kato, K. Fujiishi, M. Nagatani, *Analytical Chemistry* **1962**, *34*, 1502-1503.
[2] Y. Shimizu, M. Egashira, *MRS Bull.* **1999**, *24*, 18-24.
[3] F. Röck, N. Barsan, U. Weimar, *Chemical Reviews* **2008**, *108*, 705-725.
[4] K. S. Park, Z. Ni, A. P. Cote, J. Y. Choi, R. D. Huang, F. J. Uribe-Romo, H. K. Chae, M. O'Keeffe, O. M. Yaghi, *Proceedings of the National Academy of Sciences of the United States of America* **2006**, *103*, 10186-10191.
[5] Y. N. Xia, P. D. Yang, Y. G. Sun, Y. Y. Wu, B. Mayers, B. Gates, Y. D. Yin, F. Kim, Y. Q. Yan, *Advanced Materials* **2003**, *15*, 353-389.
[6] A. P. Alivisatos, *Science* **1996**, *271*, 933-937.
[7] J. M. Krans, J. M. van Ruitenbeek, V. V. Fisun, I. K. Yanson, L. J. de Jongh, *Nature* **1995**, *375*, 767-769.
[8] G. Markovich, C. P. Collier, S. E. Henrichs, F. Remacle, R. D. Levine, J. R. Heath, *Accounts of Chemical Research* **1999**, *32*, 415-423.
[9] A. Kolmakov, M. Moskovits, *Ann. Rev. Mater. Res.* **2004**, *34*, 151-180.
[10] S. Barth, R. Jimenez-Diaz, J. Sama, J. D. Prades, I. Gracia, J. Santander, C. Cane, A. Romano-Rodriguez, *Chem Commun (Camb)* **2012**, *48*, 4734-4736.
[11] M. S. Arnold, P. Avouris, Z. W. Pan, Z. L. Wang, *The Journal of Physical Chemistry B* **2003**, *107*, 659-663.
[12] M. H. Huang, S. Mao, H. Feick, H. Yan, Y. Wu, H. Kind, E. Weber, R. Russo, P. Yang, *Science* **2001**, *292*, 1897-1899.
[13] K. Haraguchi, T. Katsuyama, K. Hiruma, *Journal of Applied Physics* **1994**, *75*, 4220-4225.
[14] C. J. Lee, T. J. Lee, S. C. Lyu, Y. Zhang, H. Ruh, H. J. Lee, *Applied Physics Letters* **2002**, *81*, 3648-3650.
[15] B. Tian, X. Zheng, T. J. Kempa, Y. Fang, N. Yu, G. Yu, J. Huang, C. M. Lieber, *Nature* **2007**, *449*, 885-889.
[16] C. K. Chan, H. Peng, G. Liu, K. McIlwrath, X. F. Zhang, R. A. Huggins, Y. Cui, *Nat Nanotechnol* **2008**, *3*, 31-35.
[17] Z. L. Wang, J. Song, *Science* **2006**, *312*, 242-246.
[18] S. Barth, F. Hernandez-Ramirez, J. D. Holmes, A. Romano-Rodriguez, *Progress in Materials Science* **2010**, *55*, 563-627.
[19] G. Yu, A. Cao, C. M. Lieber, *Nat Nano* **2007**, *2*, 372-377.
[20] A. Javey, Nam, R. S. Friedman, H. Yan, C. M. Lieber, *Nano Letters* **2007**, *7*, 773-777.
[21] S. Raychaudhuri, S. A. Dayeh, D. Wang, E. T. Yu, *Nano Letters* **2009**, *9*, 2260-2266.
[22] T. J. Trentler, K. M. Hickman, S. C. Goel, A. M. Viano, P. C. Gibbons, W. E. Buhro, *Science* **1995**, *270*, 1791-1794.
[23] J. Wang, K. Chen, M. Gong, B. Xu, Q. Yang, *Nano Letters* **2013**, *13*, 3996-4000.
[24] J. Stejny, R. W. Trinder, J. Dlugosz, *J. Mater. Sci.* **1981**, *16*, 3161-3170.
[25] G. W. Sears, *Acta Metallurgica* **1955**, *3*, 361-366.
[26] Z. L. Wang, X. Y. Kong, J. M. Zuo, *Physical Review Letters* **2003**, *91*, 185502.
[27] F. C. Frank, *Discussions of the Faraday Society* **1949**, *5*, 48.
[28] S. Rackauskas, H. Jiang, J. B. Wagner, S. D. Shandakov, T. W. Hansen, E. I. Kauppinen, A. G. Nasibulin, *Nano Letters* **2014**, *14*, 5810-5813.
[29] L. Venkataraman, C. M. Lieber, *Physical Review Letters* **1999**, *83*, 5334-5337.
[30] B. Gates, Y. Yin, Y. Xia, *Journal of the American Chemical Society* **2000**, *122*, 12582-12583.
[31] C. J. Hawley, B. R. Beatty, G. Chen, J. E. Spanier, *Crystal Growth & Design* **2012**, *12*, 2789-2793.
[32] R. S. Wagner, W. C. Ellis, *Applied Physics Letters* **1964**, *4*, 89.
[33] H. Okamoto, T. B. Massalski, *Bulletin of Alloy Phase Diagrams* **1984**, *5*, 601-610.
[34] M. S. Seifner, F. Biegger, A. Lugstein, J. Bernardi, S. Barth, *Chem. Mat.* **2015**, *27*, 6125-6130.
[35] S. Barth, M. S. Seifner, J. Bernardi, *Chem Commun (Camb)* **2015**, *51*, 12282-12285.

[36] K. Choy, *Progress in Materials Science* **2003**, *48*, 57-170.
[37] S. L. James, *Chemical Society Reviews* **2003**, *32*, 276-288.
[38] H. Furukawa, K. E. Cordova, M. O'Keeffe, O. M. Yaghi, *Science* **2013**, *341*, 1230444.
[39] M. Eddaoudi, D. B. Moler, H. Li, B. Chen, T. M. Reineke, M. O'Keeffe, O. M. Yaghi, *Accounts of Chemical Research* **2001**, *34*, 319-330.
[40] M. Eddaoudi, J. Kim, N. Rosi, D. Vodak, J. Wachter, M. O'Keeffe, O. M. Yaghi, *Science* **2002**, *295*, 469-472.
[41] A. R. Millward, O. M. Yaghi, *Journal of the American Chemical Society* **2005**, *127*, 17998-17999.
[42] H. Wu, W. Zhou, T. Yildirim, *Journal of the American Chemical Society* **2007**, *129*, 5314-+.
[43] J. R. Li, R. J. Kuppler, H. C. Zhou, *Chemical Society Reviews* **2009**, *38*, 1477-1504.
[44] G. Lu, J. T. Hupp, *Journal of the American Chemical Society* **2010**, *132*, 7832-+.
[45] L. E. Kreno, K. Leong, O. K. Farha, M. Allendorf, R. P. Van Duyne, J. T. Hupp, *Chemical Reviews* **2012**, *112*, 1105-1125.
[46] J. Lee, O. K. Farha, J. Roberts, K. A. Scheidt, S. T. Nguyen, J. T. Hupp, *Chemical Society Reviews* **2009**, *38*, 1450-1459.
[47] K. K. Tanabe, S. M. Cohen, *Chemical Society Reviews* **2011**, *40*, 498-519.
[48] S. Kitagawa, R. Kitaura, S. Noro, *Angewandte Chemie-International Edition* **2004**, *43*, 2334-2375.
[49] R. Batten Stuart, R. Champness Neil, X.-M. Chen, J. Garcia-Martinez, S. Kitagawa, L. Öhrström, M. O’Keeffe, M. Paik Suh, J. Reedijk, in *Pure and Applied Chemistry, Vol. 85*, **2013**, p. 1715.
[50] N. Nordin, A. F. Ismail, A. Mustafa, P. S. Goh, D. Rana, T. Matsuura, *Rsc Advances* **2014**, *4*, 33292-33300.
[51] P. M. Forster, N. Stock, A. K. Cheetham, *Angew Chem Int Ed Engl* **2005**, *44*, 7608-7611.
[52] N. A. Khan, S. H. Jhung, *Crystal Growth & Design* **2010**, *10*, 1860-1865.
[53] U. Mueller, H. Puetter, M. Hesse, H. Wessel, **2005**.
[54] A. Pichon, A. Lazuen-Garay, S. L. James, *CrystEngComm* **2006**, *8*, 211-214.
[55] J. Kim, S.-T. Yang, S. B. Choi, J. Sim, J. Kim, W.-S. Ahn, *Journal of Materials Chemistry* **2011**, *21*, 3070.
[56] O. Shekhah, H. Wang, S. Kowarik, F. Schreiber, M. Paulus, M. Tolan, C. Sternemann, F. Evers, D. Zacher, R. A. Fischer, C. Woll, *Journal of the American Chemical Society* **2007**, *129*, 15118-+.
[57] O. Shekhah, H. Wang, M. Paradinas, C. Ocal, B. Schupbach, A. Terfort, D. Zacher, R. A. Fischer, C. Woll, *Nature Materials* **2009**, *8*, 481-484.
[58] O. Shekhah, H. Wang, D. Zacher, R. A. Fischer, C. Woll, *Angewandte Chemie-International Edition* **2009**, *48*, 5038-5041.
[59] O. Shekhah, L. L. Fu, R. Sougrat, Y. Belmabkhout, A. J. Cairns, E. P. Giannelis, M. Eddaoudi, *Chemical Communications* **2012**, *48*, 11434-11436.
[60] O. Shekhah, R. Swaidan, Y. Belmabkhout, M. du Plessis, T. Jacobs, L. J. Barbour, I. Pinnau, M. Eddaoudi, *Chemical Communications* **2014**, *50*, 2089-2092.
[61] O. Shekhah, M. Eddaoudi, *Chemical Communications* **2013**, *49*, 10079-10081.
[62] N. Barsan, U. Weimar, *J. Electroceram.* **2001**, *7*, 143-167.
[63] M. E. Franke, T. J. Koplin, U. Simon, *Small* **2006**, *2*, 36-50.
[64] K. L. Chopra, S. Major, D. K. Pandya, *Thin Solid Films* **1983**, *102*, 1-46.
[65] M. Batzill, U. Diebold, *Progress in Surface Science* **2005**, *79*, 47-154.
[66] B. G. Lewis, D. C. Paine, *MRS Bull.* **2000**, *25*, 22-27.
[67] N. Kruse, A. Frennet, J.-M. Bastin, *Studies in Surface Science and Catalysis* **1998**, *116*, 696.
[68] S. Mathur, S. Barth, H. Shen, J.-C. Pyun, U. Werner, *Small* **2005**, *1*, 713-717.
[69] S. Mathur, S. Barth, *Small* **2007**, *3*, 2070-2075.
[70] Y.-J. Ma, F. Zhou, L. Lu, Z. Zhang, *Solid State Communications* **2004**, *130*, 313-316.
[71] Y. Lilach, J.-P. Zhang, M. Moskovits, A. Kolmakov, *Nano Letters* **2005**, *5*, 2019-2022.
[72] Z.-G. Zhao, M. Miyauchi, *Angewandte Chemie International Edition* **2008**, *47*, 7051-7055.

[73] S. Daothong, N. Songmee, N. Dejang, T. Pichler, H. Shiozawa, Y. Jia, D. Batchelor, E. Kauppinen, S. Thongtem, P. Ayala, P. Singjai, *The Journal of Physical Chemistry C* **2010**, *114*, 10-14.

[74] Q. Sun, F. Xiao, S. Ren, Z. Dong, J. Wang, X. Su, *Ceramics International* **2014**, *40*, 11447-11451.

[75] M. Szabó, P. Pusztai, A.-R. Leino, K. Kordás, Z. Kónya, Á. Kukovecz, *Journal of Molecular Structure* **2013**, *1044*, 99-103.

[76] G. R. Bamwenda, K. Sayama, H. Arakawa, *Journal of Photochemistry and Photobiology A: Chemistry* **1999**, *122*, 175-183.

[77] C. G. Granqvist, *Solar Energy Materials and Solar Cells* **2000**, *60*, 201-262.

[78] T. Zhu, M. N. Chong, E. S. Chan, *ChemSusChem* **2014**, *7*, 2974-2997.

[79] F. E. Annanouch, I. Gràcia, E. Figueras, E. Llobet, C. Cané, S. Vallejos, *Sensors and Actuators B: Chemical* **2015**, *216*, 374-383.

[80] S. Vallejos, I. Gracia, E. Figueras, C. Cane, *Journal of Nanomaterials* **2014**, 9.

[81] M. Burdis, J. Siddle, R. Batchelor, J. Gallego, *Electrochromic device development for large scale applications, Vol. 2531*, Spie - Int Soc Optical Engineering, Bellingham, **1995**.

[82] A. K. Prasad, P. I. Gouma, *J. Mater. Sci.* **2003**, *38*, 4347-4352.

[83] V. Khatko, J. Calderer, E. Llobet, X. Correig, *Sensors and Actuators B: Chemical* **2005**, *109*, 128-134.

[84] M. Ling, C. Blackman, *Physica Status Solidi C: Current Topics in Solid State Physics, Vol 12, No 7* **2015**, *12*, 869-877.

[85] H. Kim, R. O. Bonsu, C. O'Donohue, R. Y. Korotkov, L. McElwee-White, T. J. Anderson, *Acs Applied Materials & Interfaces* **2015**, *7*, 2660-2667.

[86] J. Greil, S. Birner, E. Bertagnolli, A. Lugstein, *Applied Physics Letters* **2014**, *104*, 163901.

[87] B. A. Korgel, T. Hanrath, *Proceedings of the Institution of Mechanical Engineers, Part N: Journal of Nanoengineering and Nanosystems* **2004**, *218*, 25-34.

[88] M. H. Seo, M. Park, K. T. Lee, K. Kim, J. Kim, J. Cho, *Energy Environ. Sci.* **2011**, *4*, 425-428.

[89] B. Polyakov, B. Daly, J. Prikulis, V. Lisauskas, B. Vengalis, M. A. Morris, J. D. Holmes, D. Erts, *Advanced Materials* **2006**, *18*, 1812-+.

[90] D. M. A. Mackenzie, S. A. Brown, *Journal of Applied Physics* **2012**, *112*, 074514.

[91] J. Samà, M. S. Seifner, G. Domènech-Gil, J. Santander, C. Calaza, M. Moreno, I. Gràcia, S. Barth, A. Romano-Rodríguez, *Sensors and Actuators B: Chemical* **2017**, *243*, 669-677.

[92] G. A. Bootsma, H. J. Gassen, *J. Cryst. Growth* **1971**, *10*, 223-234.

[93] S. Barth, M. M. Koleśnik, K. Donegan, V. Krstić, J. D. Holmes, *Chem. Mat.* **2011**, *23*, 3335-3340.

[94] A. M. Chockla, B. A. Korgel, *Journal of Materials Chemistry* **2009**, *19*, 996-1001.

[95] A. M. Morales, C. M. Lieber, *Science* **1998**, *279*, 208-211.

[96] P. Nguyen, H. T. Ng, M. Meyyappan, *Advanced Materials* **2005**, *17*, 549-553.

[97] K. M. Ryan, D. Erts, H. Olin, M. A. Morris, J. D. Holmes, *Journal of the American Chemical Society* **2003**, *125*, 6284-6288.

[98] C. Fang, H. Föll, J. Carstensen, *Nano Letters* **2006**, *6*, 1578-1580.

[99] K. Persaud, G. Dodd, *Nature* **1982**, *299*, 352-355.

[100] A. D. Wilson, M. Baietto, *Sensors* **2009**, *9*, 5099-5148.

[101] R. Lucklum, P. Hauptmann, *Sensors and Actuators B: Chemical* **2000**, *70*, 30-36.

[102] J. W. Gardner, T. C. Pearce, S. Friel, P. N. Bartlett, N. Blair, *Sensors and Actuators B: Chemical* **1994**, *18*, 240-243.

[103] V. V. Sysoev, J. Goschnick, T. Schneider, E. Strelcov, A. Kolmakov, *Nano Letters* **2007**, *7*, 3182-3188.

[104] J. Puigcorbe, D. Vogel, B. Michel, A. Vila, I. Gracia, C. Cane, J. R. Morante, *Journal of Micromechanics and Microengineering* **2003**, *13*, 548-556.

[105] B. D. Sosnowchik, L. Lin, O. Englander, *Journal of Applied Physics* **2010**, *107*, 051101.

[106] J. H. Woodruff, J. B. Ratchford, I. A. Goldthorpe, P. C. McIntyre, Chidsey, *Nano Letters* **2007**, *7*, 1637-1642.

[107] G. Dubey, G. P. Lopinski, F. Rosei, *Applied Physics Letters* **2007**, *91*, 232111.

[108] L. Zhu, S. Saha, Y. Wang, D. A. Keszler, C. Fang, *The Journal of Physical Chemistry B* **2016**, *120*, 13161-13168.

[109] E. Ö. Üstün, C. Kaya, *Journal of Molecular Structure: THEOCHEM* **2004**, *710*, 133-137.

[110] Y. Zhou, W. Wu, G. Hu, H. Wu, S. Cui, *Mater. Res. Bull.* **2008**, *43*, 2113-2118.

[111] W. W. Zhan, Q. Kuang, J. Z. Zhou, X. J. Kong, Z. X. Xie, L. S. Zheng, *Journal of the American Chemical Society* **2013**, *135*, 1926-1933.

[112] M. Drobek, J. H. Kim, M. Bechelany, C. Vallicari, A. Julbe, S. S. Kim, *ACS Appl. Mater. Interfaces* **2016**, *8*, 8323-8328.

[113] M. Drobek, M. Bechelany, C. Vallicari, A. Abou Chaaya, C. Charmette, C. Salvador-Levehang, P. Miele, A. Julbe, *Journal of Membrane Science* **2015**, *475*, 39-46.

[114] H. Al-Kutubi, A. Dikhtiarenko, H. R. Zafarani, E. J. R. Sudhölter, J. Gascon, L. Rassaei, *CrystEngComm* **2015**, *17*, 5360-5364.

[115] K. Khaletskaya, S. Turner, M. Tu, S. Wannapaiboon, A. Schneemann, R. Meyer, A. Ludwig, G. Van Tendeloo, R. A. Fischer, *Advanced Functional Materials* **2014**, *24*, 4804-4811.